http://www.aimspress.com/journal/mine

Mathematics in Engineering, 8(3): 340–367.
DOI:10.3934/mine.2026011
Received: 28 April 2025
Revised: 12 November 2025
Accepted: 26 March 2026
Published: 01 May 2026

Research article

Dynamics of a 3D leader-follower system coupled via friction interface

D. Rachinskii[1,*], **M. Ruderman**[2] **and A. Zagvozdkin**[3]

[1] Department of Mathematical Sciences, The University of Texas at Dallas, USA
[2] Department of Engineering Sciences, University of Agder, Norway
[3] Department of Statistics, Virginia Tech University, USA

* **Correspondence:** Email: dmitry.rachinskiy@utdallas.edu.

Abstract: We consider dynamics of an oscillatory mechanical system with 1.5 degrees of freedom. The system consists of two linear subsystems, a leader and a follower, which are coupled via a kinetic friction interface, and additionally driven by a proportional control term. The kinetic friction model accounts for the Coulomb friction and the Stribeck effect (as negative damping) at the passage from zero to nonzero relative velocity. The equations of motion are equivalent to a Lur'e system with a single sign nonlinearity. We show that at a critical value of the parameter the zero steady state blows up into an attracting continuum (segment) of equilibrium states. Moreover, two antipodal small-amplitude periodic orbits bifurcate from the end points of the segment of equilibrium states, creating stick-slip vibrations. We consider other possible attractors consisting of stick-slip solutions of the Lur'e system such as a $\mathbb{Z}_2$-symmetric stick-slip periodic orbit and an attractor composed of a continuum of heteroclinic loops representing stick-slip motions towards a steady state.

Keywords: Coulomb friction; Stribeck effect; Lur'e system; Filippov's system; Hopf bifurcation; stick-slip periodic motion; attractor

1. Introduction

The motion of two inertial bodies connected via a passive frictional contact is a non-trivial problem (e.g., [34]) with a wide range of system and control applications. This setting is exceedingly common in processing and manufacturing on conveyor lines and turntables, material flow of items, surface treatment, preparation of mixed and shaken substances, and robot handling of free (i.e., not flanged) objects. A typical example can be a periodic controlled motion of a body placed on a driven surface. The control objective is then to navigate the system to, and maintain it in, a region of control tolerance surrounding a periodic orbit. Similar control problems have been extensively studied for rigid bodies and multi-body systems with elastic connections [1,17,28,31] including energy dissipation and energy

transfer aspects [18, 41]. On the other hand, to the best of our knowledge, controlled motion towards a setpoint reference and along a target trajectory has remained largely unexplored when objects are connected solely via a frictional interface.

In this work, we consider two inertial bodies with a free (of additional constraints) friction interface. We assume the classical Coulomb friction with discontinuity at the relative velocity zero crossing combined with a negative viscous friction term which accounts for the Stribeck effect at the transition from static (i.e., at zero velocity) to kinetic steady friction. An illustrative exemple is a mechanical linear oscillator with a frictionally coupled second mass, see Figure 1. As such, the system has one active degree of freedom (the driving body, m_2) and one passive degree of freedom (the driven body, m_1) resulting in a 3-dimensional state (phase) space, because the forces depend on the position and velocity of the driven body and the velocity of the driving body but not on the position of the latter. The free system dynamics with no external excitation forces (and without velocity-weakening) converges to an equilibrium [34]. We introduce a linear feedback control $u = ax_1$ and present a case study of dynamic and bifurcation scenarios for the controlled system, which is set up as the Lur'e feedback system with the sign nonlinearity interpreted in Filippov's sense [16].

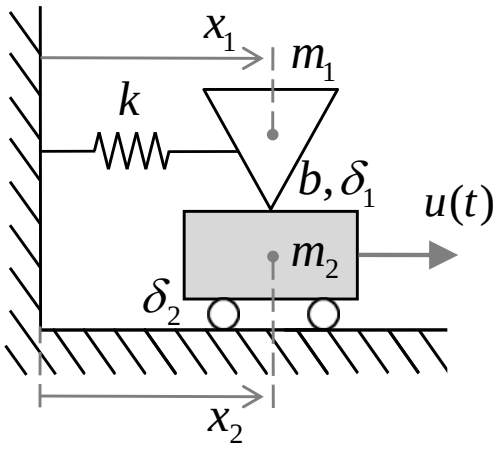

Figure 1. Two inertial bodies with a frictional interface.

Distinctive dynamic scenarios specific to Filippov's, piecewise linear, piecewise smooth and switched systems, in particular discontinuity-induced bifurcations of sliding modes [7, 20], have been extensively studied since the second half of 1990s (we refer to surveys [14, 25, 27], see also [6, 21, 24, 37]) on the basis of important earlier results [4, 15, 16, 40]. In our case, stick-slip motions correspond to the trajectories which partly belong to the sliding region located within a two-dimensional switching plane. We analyze dynamics using a one-dimensional Poincaré map defined on a part of the boundary (exit set) of the sliding region. This Poincaré map can have discontinuities. Hence, we derive sufficient conditions for the continuity on specified intervals and obtain the existence of periodic orbits from the intermediate value theorem. The basic bifurcation scenario is similar to the one shown in [26] for a 3D continuous piecewise smooth system. This scenario is associated with the discontinuity and $\mathbb{Z}_2$ antipodal symmetry of the system. More precisely, a stable steady state blows up to an attracting continuum of steady states at the critical value of the parameter with two antipodal stick-slip periodic orbits bifurcating from the end points of this continuum as the parameter crosses the

critical value. Alternative and additional attractors of the Lur'e system include a $\mathbb{Z}_2$-symmetric stick-slip periodic orbit and an attractor consisting of stick-slip homoclinic trajectories. Bifurcations from the end points of a continuum of equilibrium states are typical of systems with frictions [8]. On the other hand, frequency criteria which ensure the global stability of the equilibrium set, thus excluding any non-stationary attractors, have been studied in [44].

The paper is organized as follows. Section 2 introduces a motivating example of a leader-follower system with a dry friction interface and an equivalent piecewise linear 3D Lur'e system with the sign discontinuity. Section 3 contains the main results. In Section 3.1, we formulate the assumptions and introduce a rescaled form of the Lur'e system with a reduced number of parameters, which is used throughout the rest of the paper. In Section 3.2, the switching surface, the sliding region and switched dynamics are discussed. Section 3.3 discusses the equilibrium set and its stability depending on the system parameters, and the associated pitchfork-type bifurcation of equilibrium states. Section 3.4 presents sufficient conditions for the bifurcation of two switched periodic orbits from the continuum of equilibrium states. Other attracting sets of the system are discussed in Section 3.5. In Section 4, we introduce the one-dimensional Poincaré map as the main analysis tool. Section 5 presents numerical examples of different attracting sets and the corresponding Poincaré maps. The proofs are presented in the appendix.

2. Motivating example

2.1. A leader-follower system with a dry friction interface

Let us consider a leader-follower configuration of two linear one-degree-of-freedom systems coupled via a dry friction interface, see Figure 1. Before the systems are coupled, the follower system is a harmonic spring-mass oscillator:

$$m_1\ddot{x}_1 + kx_1 = 0,$$

where m_1 is the mass and k is the stiffness of a mechanical spring connecting the follower system to a common ground, the configuration which appears in mechanisms with restoring forces and flexible fixture structures. The equation of motion of the leader system is

$$m_2\ddot{x}_2 + \delta_2\dot{x}_2 = u(t),$$

where m_2 is the mass, δ_2 is the viscous friction coefficient and $u(t)$ is the control input. At the dry friction interface, we assume the Coulomb friction combined with a negative viscous friction term which accounts for the Stribeck effect. This results in the coupled system

$$\begin{aligned} m_1\ddot{x}_1 + kx_1 &= \delta_1(\dot{x}_1 - \dot{x}_2) - b\,\mathrm{sign}\,(\dot{x}_1 - \dot{x}_2), \\ m_2\ddot{x}_2 + \delta_2\dot{x}_2 &= u(t) - \delta_1(\dot{x}_1 - \dot{x}_2) + b\,\mathrm{sign}\,(\dot{x}_1 - \dot{x}_2), \end{aligned} \tag{2.1}$$

where all the parameters are positive.

2.2. Equivalent Lur'e system

In what follows, we consider system (2.1) with the proportional feedback control $u = ax_1$, i.e., the closed-loop system

$$\begin{aligned} m_1\ddot{x}_1 + kx_1 &= \delta_1(\dot{x}_1 - \dot{x}_2) - b\,\mathrm{sign}\,(\dot{x}_1 - \dot{x}_2), \\ m_2\ddot{x}_2 + \delta_2\dot{x}_2 &= ax_1 - \delta_1(\dot{x}_1 - \dot{x}_2) + b\,\mathrm{sign}\,(\dot{x}_1 - \dot{x}_2). \end{aligned} \tag{2.2}$$

Since the system (2.2) does not contain the variable x_2, its dynamics can be considered in the 3-dimensional state space of the variables

$$x_1, \quad v_1 = \dot{x}_1, \quad v_2 = \dot{x}_2.$$

Specifically, using the notation $\boldsymbol{z}_m = (x_1, v_1, v_2)^T$ for the state vector (where ^{T} denotes the transposition), the system (2.2) is equivalent to

$$\dot{\boldsymbol{z}}_m = A_m\boldsymbol{z}_m + \boldsymbol{b}_m\,\mathrm{sign}\,(\boldsymbol{c}_m^T\boldsymbol{z}_m), \tag{2.3}$$

where

$$A_m = \begin{bmatrix} 0 & 1 & 0 \\ -k/m_1 & \delta_1/m_1 & -\delta_1/m_1 \\ a/m_2 & -\delta_1/m_2 & (\delta_1 - \delta_2)/m_2 \end{bmatrix}, \ \boldsymbol{b}_m = \begin{bmatrix} 0 \\ b/m_1 \\ -b/m_2 \end{bmatrix}, \ \boldsymbol{c}_m = \begin{bmatrix} 0 \\ -1 \\ 1 \end{bmatrix}. \tag{2.4}$$

We assume that

$$a > -(\delta_2 - \delta_1)\frac{k}{\delta_1}, \qquad a > -\frac{km_2 - \delta_1\delta_2}{m_1} - (\delta_2 - \delta_1)\frac{\delta_2}{m_1}. \tag{2.5}$$

These conditions ensure that the matrix A_m has one negative eigenvalue and two unstable eigenvalues.

Moreover, we assume that the unstable eigenvalues are complex.

Remark 2.1. *Condition* (2.5) *is satisfied for $a \geq 0$ if $\delta_1 < \delta_2$. Moreover, by inspection, if $\delta_1^2 \ll km_1$, then A_m has a complex conjugate pair of unstable eigenvalues because the spectrum of A_m for $\delta_1 = 0$ is $-\delta_2/m_2$, $\pm i\sqrt{k/m_1}$.*

3. Main results

3.1. Assumptions

Let us consider the system

$$\dot{\boldsymbol{z}} = A\boldsymbol{z} + \boldsymbol{b}\,\mathrm{sign}\,(\langle \boldsymbol{c}, \boldsymbol{z}\rangle) \tag{3.1}$$

with the state $\boldsymbol{z} \in \mathbb{R}^3$, where $\langle\cdot,\cdot\rangle$ denotes a linear functional on $\mathbb{R}^3$ (cf. (2.3)).

Assume that A is a non-singular linear map (square matrix) with a pair of complex eigenvalues $\alpha' \pm i\beta'$ corresponding to complex eigenvectors $\boldsymbol{u}_1 \pm i\boldsymbol{u}_2$ ($\boldsymbol{u}_1, \boldsymbol{u}_2 \in \mathbb{R}^3$) and a real eigenvalue γ' corresponding to a real eigenvector $\boldsymbol{u}_3 \in \mathbb{R}^3$, i.e.,

$$A\boldsymbol{u}_1 = \alpha'\boldsymbol{u}_1 - \beta'\boldsymbol{u}_2, \qquad A\boldsymbol{u}_2 = \beta'\boldsymbol{u}_1 + \alpha'\boldsymbol{u}_2, \qquad A\boldsymbol{u}_3 = \gamma'\boldsymbol{u}_3. \tag{3.2}$$

We require that

$$\alpha' > 0, \quad \beta' > 0, \quad \gamma' < 0 \tag{3.3}$$

and

$$\langle \boldsymbol{c}, \boldsymbol{b} \rangle < 0. \tag{3.4}$$

We further require that system (3.1) is observable:

$$\text{functionals } \boldsymbol{c}, A^*\boldsymbol{c}, (A^*)^2\boldsymbol{c} \text{ are linearly independent,} \tag{3.5}$$

where A^* is the adjoint for A. The following two quantities will play an important role:

$$\sigma := \langle \boldsymbol{c}, A^{-1}\boldsymbol{b} \rangle, \qquad \kappa := \langle \boldsymbol{c}, A^{-2}\boldsymbol{b} \rangle. \tag{3.6}$$

Remark 3.1. *By a linear scaling of time, one can ensure that the spectrum of A is $\{\alpha \pm i, \gamma\}$, where*

$$\alpha = \frac{\alpha'}{\beta'} > 0, \qquad \gamma = \frac{\gamma'}{\beta'} < 0. \tag{3.7}$$

Moreover, a proper rescaling of the functional $\boldsymbol{c}$ transforms (3.4) *into*

$$\langle \boldsymbol{c}, \boldsymbol{b} \rangle = -1. \tag{3.8}$$

This transformed version of system (3.1) *is used everywhere below. Condition* (3.4) *is discussed in the next subsection.*

We will use the following canonical coordinate form of system (3.1) with the matrix in the companion form (see, for example, [11]). The observability condition (3.5) ensures that the functionals

$$\boldsymbol{c}_s^{(1)} = \boldsymbol{c}, \quad \boldsymbol{c}_s^{(2)} = (A^*)^{-1}\boldsymbol{c}, \quad \boldsymbol{c}_s^{(3)} = (A^*)^{-2}\boldsymbol{c} \tag{3.9}$$

form a basis in the dual space. Let $\boldsymbol{b}_s^{(i)}$, $i = 1, 2, 3$, be the dual basis for (3.9), i.e.,

$$\langle \boldsymbol{c}_s^{(i)}, \boldsymbol{b}_s^{(j)} \rangle = \delta_{ij}. \tag{3.10}$$

The coordinate form of system (3.1) in these bases can be obtained from the Cayley–Hamilton theorem, i.e.,

$$A^3 - (2\alpha + \gamma)A^2 + (\alpha^2 + 2\alpha\gamma + 1)A - \gamma(\alpha^2 + 1)I = 0 \tag{3.11}$$

with I denoting the identity matrix implies

$$A = \begin{bmatrix} 2\alpha + \gamma & -(1 + \alpha^2 + 2\alpha\gamma) & \gamma(1 + \alpha^2) \\ 1 & 0 & 0 \\ 0 & 1 & 0 \end{bmatrix}, \quad \boldsymbol{b} = \begin{bmatrix} -1 \\ \sigma \\ \kappa \end{bmatrix}, \quad \boldsymbol{c} = \begin{bmatrix} 1 \\ 0 \\ 0 \end{bmatrix} \tag{3.12}$$

with $\langle \boldsymbol{c}, z \rangle = \boldsymbol{c}^T z = \sum_{i=1}^3 c_i z_i$. Everywhere below, we identify system (3.1) with this coordinate form. We use the notation $\Theta : \mathbb{R}_+ \times \mathbb{R}^3 \to \mathbb{R}^3$ for the flow of system (3.1), i.e., $z(t) = \Theta(t, z')$ is the solution of system (3.1) with the initial value

$$z(0) = z'. \tag{3.13}$$

Remark 3.2. *From relation* (2.4)*, it follows that the leader-follower system* (2.2) *satisfies condition* (3.4) *and for this system*

$$\sigma = \frac{b(k - a)}{k\delta_2 + (a - k)\delta_1}, \tag{3.14}$$

$$\kappa = \frac{bk(\delta_2^2 + m_2(a - k))}{(k\delta_2 + (a - k)\delta_1)^2}. \tag{3.15}$$

3.2. Preliminaries: switching surface and sliding region

The phase space of system (3.1) is divided by the *switching surface* (plane)

$$S = \{z \in \mathbb{R}^3 : \boldsymbol{c}^T z = 0\}$$

separating the half-spaces

$$\Omega_- = \{z \in \mathbb{R}^3 : \boldsymbol{c}^T z < 0\}; \qquad \Omega_+ = \{z \in \mathbb{R}^3 : \boldsymbol{c}^T z > 0\}.$$

The velocity field of system (3.1) equals

$$\Phi_-(z) = Az - \boldsymbol{b} \quad \text{in} \quad \Omega_-; \qquad \Phi_+(z) = Az + \boldsymbol{b} \quad \text{in} \quad \Omega_+ \tag{3.16}$$

with a discontinuity on S. In order to describe the switching behavior of trajectories, we consider three parts of the switching plane S:

$$S_- = \left\{z \in S : \boldsymbol{c}^T Az < -1\right\}, \qquad S_+ = \left\{z \in S : \boldsymbol{c}^T Az > 1\right\}, \tag{3.17}$$

$$S_0 = \left\{z \in S : \left|\boldsymbol{c}^T Az\right| < 1\right\}. \tag{3.18}$$

Hence,

$$S = \overline{S_-} \cup S_0 \cup \overline{S_+},$$

where $\overline{S_\pm}$ denotes the closure of $S_\pm$. From the observability assumption (3.5), it follows that $S_\pm$ are not empty. By inspection, the vector fields $\Phi_\pm$ satisfy

$$\boldsymbol{c}^T\Phi_\pm > 0 \ \text{ on } \ S_+; \qquad \boldsymbol{c}^T\Phi_\pm < 0 \ \text{ on } \ S_-; \tag{3.19}$$

$$\boldsymbol{c}^T\Phi_- > 0, \ \ \boldsymbol{c}^T\Phi_+ < 0 \ \text{ on } \ S_0, \tag{3.20}$$

where

$$\boldsymbol{n}_S = \boldsymbol{c}/\left|\boldsymbol{c}\right| \tag{3.21}$$

is the normal unit vector to S pointing from Ω_- to Ω_+. Therefore, $S_\pm$ are the so-called *crossing regions* and the part S_0 of S is the so-called *sliding region* [1, 16].

Condition (3.4) ensures that the sliding region S_0 is *attracting*. Indeed, from (3.1), it follows that

$$\frac{1}{2}\frac{d}{dt}\left(\boldsymbol{c}^T z\right)^2 = \left(\boldsymbol{c}^T z\right)\, \boldsymbol{c}^T Az + \left|\boldsymbol{c}^T z\right|\, \boldsymbol{c}^T \boldsymbol{b},$$

hence the relation $\boldsymbol{c}^T\boldsymbol{b} = -1$ (cf. (3.8), which is equivalent to (3.4)) implies that

$$\frac{d}{dt}(\boldsymbol{c}^T z)^2 < 0 \quad \text{if} \quad \left|\boldsymbol{c}^T Az\right| < 1, \ z \notin S.$$

By the same token, the inequality $\langle \boldsymbol{c}, \boldsymbol{b}\rangle > 0$, which is opposite to (3.4), makes the sliding region repelling.

The sliding region S_0 consists of the trajectories, and parts thereof, known as *sliding modes* in Filippov's sense [16]. In particular, the flow in the sliding region S_0 follows the equation

$$\dot{z} = Bz, \quad z \in S_0, \tag{3.22}$$

where

$$B = \left(I + \boldsymbol{b}\boldsymbol{c}^T\right) A. \tag{3.23}$$

Notice that the switching plane S is an invariant subspace for B and $I + \boldsymbol{b}\boldsymbol{c}^T$ is the linear projection onto S along the vector $\boldsymbol{b}$ due to $\boldsymbol{c}^T\boldsymbol{b} = -1$ (cf. (3.8)). Moreover, $A^{-1}\boldsymbol{b}$ is an eigenvector of B with the zero eigenvalue, the matrix B is singular, and, from $\operatorname{rank}(\boldsymbol{b}\boldsymbol{c}^T) = 1$ and $\det A \neq 0$, it follows that $\operatorname{rank}\left(I + \boldsymbol{b}\boldsymbol{c}^T\right) \geq 2$. Hence,

$$\operatorname{rank} B = 2. \tag{3.24}$$

From (3.12), it follows that in the basis $\boldsymbol{b}_s^{(i)}$ (cf. (3.9) and (3.10)),

$$B = \begin{bmatrix} 0 & 0 & 0 \\ 1 + \sigma(2\alpha + \gamma) & -\sigma(1 + \alpha^2 + 2\alpha\gamma) & \sigma\gamma(1 + \alpha^2) \\ \kappa(2\alpha + \gamma) & 1 - \kappa(1 + \alpha^2 + 2\alpha\gamma) & \kappa\gamma(1 + \alpha^2) \end{bmatrix}.$$

Therefore, the trace and determinant of the restriction of B to S are given by

$$\operatorname{tr}(B|_S) = (1 + \alpha^2)\gamma\kappa - \sigma(1 + \alpha^2 + 2\alpha\gamma), \tag{3.25}$$

$$\det(B|_S) = -(1 + \alpha^2)\gamma\sigma. \tag{3.26}$$

In particular, if $\sigma = 0$ and $\kappa \neq 0$, then the restriction $B|_S$ has the eigenvalues

$$\lambda_1 = 0, \quad \lambda_2 = (1 + \alpha^2)\gamma\kappa \tag{3.27}$$

with the corresponding eigenvectors

$$\boldsymbol{v}_1 = -\kappa\boldsymbol{b}_s^{(2)} + \frac{1 - \kappa(\alpha^2 + 1 + 2\alpha\gamma)}{\gamma(\alpha^2 + 1)}\boldsymbol{b}_s^{(3)} = -A^{-1}\boldsymbol{b}, \tag{3.28}$$

$$\boldsymbol{v}_2 = \frac{1}{\gamma(\alpha^2 + 1)}\boldsymbol{b}_s^{(3)}. \tag{3.29}$$

If $\sigma = 0$ and $\kappa = 0$, then $\lambda_1 = \lambda_2 = 0$, vectors (3.28) and (3.29) coincide, and $B|_S$ has a generalized eigenvector $\boldsymbol{v}^g = \frac{1}{\gamma(\alpha^2+1)}\boldsymbol{b}_s^{(2)} \in S$, i.e.,

$$B\boldsymbol{v}^g = \boldsymbol{v}_1 = \boldsymbol{v}_2, \quad B\boldsymbol{v}_2 = 0 \quad \text{if} \quad \sigma = \kappa = 0. \tag{3.30}$$

Remark 3.3. *From Remark 3.2, it follows that for system* (2.2)*,*

$$\operatorname{tr}(B|_S) = \frac{\delta_1 - \delta_2}{m_1 + m_2}, \quad \det(B|_S) = \frac{k - a}{m_1 + m_2}.$$

3.3. Stability of equilibrium states

Let us consider equilibrium states of system (3.1).

Theorem 3.1. *System* (3.1) *has the following equilibria:*

(i) *For $\sigma > 0$, system* (3.1) *has a unique zero equilibrium $\boldsymbol{z}_*^0 = 0$. This equilibrium belongs to the sliding region S_0. If $\operatorname{tr}(B|_s) < 0$, then the zero equilibrium is asymptotically stable (cf.* (3.25)*). If $\operatorname{tr}(B|_s) = 0$, then the zero equilibrium is Lyapunov stable. If $\operatorname{tr}(B|_s) > 0$, then the zero equilibrium is unstable.*

(ii) *For $\sigma = 0$, the equilibrium set of system* (3.1) *is the segment*

$$L := \{z_*^\xi = \xi \boldsymbol{d}_0 : -1 \le \xi \le 1\}, \tag{3.31}$$

where

$$\boldsymbol{d}_0 = -A^{-1}\boldsymbol{b}, \tag{3.32}$$

which, except for its end points $z_*^\pm = \pm \boldsymbol{d}_0$, belongs to the sliding region S_0 of the switching plane. If $\kappa > 0$, i.e.,

$$\operatorname{tr}(B|_s) = (1 + \alpha^2)\gamma\kappa < 0,$$

then all the equilibrium states (3.31) *are Lyapunov stable and the equilibrium set* (3.31) *is attracting. Otherwise, all the equilibrium states are unstable.*

(iii) *For $\sigma < 0$, system* (3.1) *has three equilibrium states, $z_*^0 = 0 \in S_0$ and $z_*^\pm = \pm \boldsymbol{d}_0 \in \Omega_\pm$, which are all unstable.*

The proof is presented in Appendix A.

At the zero equilibrium state of system (2.2) both masses are at rest and all the forces are zero. According to Theorem 3.1, (2.5), and (3.14), this is a unique equilibrium state for $a < k$ (recall that a measures the feedback strength). Moreover, this equilibrium is stable if $\delta_2 > \delta_1$, i.e., the coefficient of positive friction is greater than the coefficient of the negative friction.

For the critical case $a = k$, each point of the equilibrium set (3.31) corresponds to an equilibrium state of system (2.2) with both masses at rest. The spring force acting on the mass m_1 and the opposite force applied to the mass m_2 due to the feedback are compensated by the (static) dry friction between the masses. According to part (ii) of Theorem 3.1, the equilibrium set is stable (attracting) if $\delta_2 > \delta_1$.

For $a > k$, at each of the equilibrium states $z_*^\pm$, the mass m_1 is at rest while the mass m_2 is in uniform motion. The spring force is compensated by the (kinetic) dry friction. These equilibrium states are unstable. The switching surface S of system (2.2) is defined by the condition $v_1 = v_2$. In particular, during the motions corresponding to sliding modes (a trajectory, or a part thereof, that belongs to the switching region S_0), the inertial bodies stick to each other, i.e., their relative velocity is zero. On the other hand, when the relative velocity is non-zero, i.e., the inertial bodies slip against each other, the corresponding part of a trajectory belongs to $\Omega_- \cup \Omega_+$.

3.4. Bifurcation of periodic orbits from equilibrium set

Let us consider a variant of system (3.1), which continuously depends on a scalar parameter μ:

$$\dot{z} = A(\mu)z + \boldsymbol{b}(\mu)\operatorname{sign}(\langle \boldsymbol{c}(\mu), z\rangle), \qquad z \in \mathbb{R}^3,\ \mu \in (\mu_l, \mu_r)\,. \tag{3.33}$$

By $\Theta_\mu : \mathbb{R}_+ \times \mathbb{R}^3 \to \mathbb{R}^3$ we denote the flow of system (3.33).

Assume that for each $\mu \in (\mu_l, \mu_r)$ relations (3.4) and (3.5) hold and the matrix $A(\mu)$ has a negative real eigenvalue and a pair of unstable complex eigenvalues (cf. (3.3)). Using Remark 3.1, we assume without loss of generality that the eigenvalues of $A(\mu)$ are $\gamma(\mu)$, $\alpha(\mu) \pm i$, where $\alpha, \gamma : (\mu_l, \mu_r) \to \mathbb{R}$ are continuous functions and

$$\alpha(\mu) > 0, \quad \gamma(\mu) < 0, \quad \langle \boldsymbol{c}, \boldsymbol{b}(\mu)\rangle = -1, \quad \mu \in (\mu_l, \mu_r).$$

Following (3.6), define

$$\sigma(\mu) := \left\langle \boldsymbol{c}, A^{-1}(\mu)\boldsymbol{b}(\mu) \right\rangle, \quad \kappa(\mu) := \left\langle \boldsymbol{c}, A^{-2}(\mu)\boldsymbol{b}(\mu) \right\rangle. \tag{3.34}$$

Theorem 3.2. *Assume that the function $\sigma(\mu)$ defined by* (3.34) *strictly decreases and has a zero μ_o on the interval (μ_ℓ, μ_r), i.e., $\sigma(\mu_o) = 0$. Suppose that either $\alpha(\mu_o) \geq \sqrt{3}$, $\gamma(\mu_o) < 0$ or $1 < \alpha(\mu_o) < \sqrt{3}$ and*

$$\gamma(\mu_o) < \frac{\alpha(\mu_o)(\alpha^2(\mu_o) - 3)}{(\alpha^2(\mu_o) - 1)}.$$

Suppose $\kappa(\mu_o) > 0$. Then, there exists a $\mu^* \in (\mu_o, \mu_r)$ such that for any $\mu \in (\mu_o, \mu^*)$ system (3.33) *has a periodic orbit $L^H = \{z_H(t,\mu) : t \in \mathbb{R}\}$. Part of this periodic orbit belongs to $\overline{S_0}$, the other part to Ω_+. Moreover,*

$$\lim_{\mu \to \mu_o +} \max_{t \in \mathbb{R}} |z_H(t,\mu) + A^{-1}(\mu_o)\boldsymbol{b}(\mu_o)| = 0. \tag{3.35}$$

The proof of Theorem 3.2 is presented in Appendix B.

For system (2.2), the bifurcation point μ_o corresponds to $a = k$ and the condition $\kappa(\mu_o) > 0$ is satisfied in accordance with (3.15).

According to (3.35), a family of small-amplitude periodic orbits (of solutions $z_H(t,\mu)$) bifurcates from the equilibrium $\boldsymbol{d}_0(\mu_o) = -A^{-1}(\mu_o)\boldsymbol{b}(\mu_o)$ (cf. (3.32)), with the orbits approaching the equilibrium as the bifurcation parameter $\mu > \mu_o$ tends to the critical value μ_o. The following remarks provide more details of the bifurcation scenario associated with this transitioning from a steady state to small-amplitude periodic oscillations.

Remark 3.4. *Since a part of the periodic orbit L^H belongs to S_0, while the other part belongs to $\Omega_\pm$, for system* (2.2)*, solutions $z_H(t,\mu)$ correspond to stick-slip periodic motions.*

Remark 3.5. *Since system* (3.33) *is equivariant with respect to the antipodal $\mathbb{Z}_2$-action $z \to -z$, with every orbit $z(t)$ this system has an orbit $-z(t)$. Hence, under the conditions of Theorem 3.2, there are two periodic orbits $\pm z_H(t,\mu)$ for $\mu \in (\mu_o, \mu^*)$, which are different due to* (3.35).

Remark 3.6. *Assuming that the assumptions of Theorem 3.2 hold and combining it with Theorem 3.1, we see that system* (3.33) *undergoes a bifurcation scenario involving a simultaneous bifurcation of equilibrium states and small-amplitude cycles, and somewhat resembles a pitchfork bifurcation of steady states simultaneous with a $\mathbb{Z}_2$-symmetric Hopf bifurcation at $\mu = \mu_o$. Specifically, for $\mu < \mu_o$, the equilibrium at zero is attracting. At the bifurcation point $\mu = \mu_o$, it blows up to the attracting segment L of equilibrium states defined by* (3.31)*. As μ crosses the bifurcation point to the domain $\mu > \mu_o$, two unstable equilibrium states and two small periodic orbits (cycles) simultaneously bifurcate from the ends of the segment L, the equilibrium at zero becomes unstable, and the other equilibrium states disappear. The small cycles contain sliding modes. This scenario is induced by the discontinuity of system* (3.33) *and its $\mathbb{Z}_2$-symmetry.*

3.5. Attractors for $\sigma = 0$

In this section, we consider dynamics of system (3.1) for $\sigma = 0$. This corresponds to the bifurcation point $\mu = \mu_o$ for system (3.33) under the assumptions of Theorem 3.2.

Remark 3.7. *According to* (3.14)*, for system* (2.2)*,* $\sigma = 0$ *is equivalent to* $k = a$*. In other words, the external force* ax_1 *applied to the mass* m_2 *due to the feedback and the spring force* $-kx_1$ *acting on the mass* m_1 *have the same magnitude but opposite signs.*

We will consider three types of attracting sets including the segment L of equilibrium states (cf. (3.31)), a larger set $L' \supset L$ of trajectories starting from a part of the sliding region and a periodic orbit L^O defined below. We use Ruelle's definition of an attracting set [35], which coincides with Milnor's attractor [29] for L and L^O but differs for L' (see Remark 3.8 below).

Definition 3.1. A closed bounded set $\mathcal{A} \subset \mathbb{R}^3$ is called an *attracting set* if $\Theta(t, \mathcal{A}) = \mathcal{A}$ for all $t > 0$ and there is a neighborhood U of $\mathcal{A}$ such that for every neighborhood V of $\mathcal{A}$ there is a $T > 0$ such that $\Theta(t, z) \in V$ for all $z \in U$, $t > T$, where $\Theta(\cdot, \cdot)$ is the flow of system (3.1) (see Section 3.1). An attracting set $\mathcal{A}$ is called *an attractor* if no proper (non-empty) subset of $\mathcal{A}$ is an attracting set.

For the next theorem, some notation is required. Define $T^r = T^r(\alpha, \gamma)$ as the least positive root of the equation

$$f(\alpha, \gamma, T^r) = 0, \tag{3.36}$$

where

$$f(\alpha, \gamma, T) := e^{(\gamma-\alpha)T} - \cos(T) + (\alpha - \gamma)\sin(T). \tag{3.37}$$

Put

$$\rho = \rho(\alpha, \gamma) := e^{\gamma T^r} - \gamma e^{\alpha T^r} \sin(T^r), \tag{3.38}$$

$$\kappa_* = -\frac{\rho e^{-\alpha T^r}}{\gamma(\alpha^2 + 1)\sin(T^r)}, \qquad \kappa^* = -\frac{(1+\rho)e^{-\alpha T^r}}{\gamma(\alpha^2 + 1)\sin(T^r)}. \tag{3.39}$$

By inspection, $T^r \in (\pi, 2\pi)$, hence $\rho < 1$ and $\kappa^* < \kappa_* < 0$.

Define the vector $\boldsymbol{w}$ by the equations

$$\langle \boldsymbol{c}, \boldsymbol{w} \rangle = 0, \quad \langle \boldsymbol{c}, A\boldsymbol{w} \rangle = 0, \quad \left\langle \boldsymbol{c}, A^2\boldsymbol{w} \right\rangle = 1. \tag{3.40}$$

Set

$$\phi_0 = \kappa\gamma(\alpha^2 + 1) \tag{3.41}$$

and consider the parallelogram

$$N(-\phi_0, \phi_0) = \{z = \phi\boldsymbol{w} + \zeta A\boldsymbol{w} : -\phi_0 < \phi < \phi_0,\ -1 < \zeta < 1\} \subset S_0 \tag{3.42}$$

and the sets

$$L' = \overline{N(-\phi_0, \phi_0)} \cup \{\pm\Theta(t, \phi\boldsymbol{w} + A\boldsymbol{w}) : \phi \in [-\phi_0, \phi_0], t \in [0, T^r]\}, \tag{3.43}$$

$$L^O = \{\Theta(t, \boldsymbol{d}_0 + \psi^*\boldsymbol{w}) : t \geq 0\}, \tag{3.44}$$

where

$$\psi^* = \frac{2\phi_0}{1+\rho} = \frac{2\kappa\gamma(\alpha^2+1)}{1+\rho}. \tag{3.45}$$

Theorem 3.3. *Let* $\sigma = 0$.

(i) *If either* $\kappa = 0$ *and* $\rho > -1$ *or* $\kappa > 0$*, then the segment of equilibrium states* L *defined by* (3.31) *is an attractor of system* (3.1).

(ii) *If $\kappa_* \le \kappa < 0$ and $\rho > 0$, then the set L' is an attractor of system* (3.1).

(iii) *If either $\kappa^* < \kappa < \kappa_*$ and $\rho > 0$ or $\kappa^* < \kappa < 0$ and $-1 < \rho \le 0$, then L^O is an attracting periodic orbit. Part of this orbit belongs to $\overline{S_0}$, the other part belongs to $\Omega_+ \cup \Omega_-$.*

The proof is presented in Appendix C.

Statement (i) of Theorem 3.3 extends statement (ii) of Theorem 3.1. In particular, if $\kappa = 0$ and $\rho > -1$, then each equilibrium is unstable but the equilibrium set L is attracting.

As shown in the proof of part (ii), in the case $\kappa = \kappa_*$, $\rho > 0$, the attracting set L' is a union of heteroclinic trajectories and equilibrium states.

The periodic orbit L^O guaranteed by statement (iii) is different from the periodic orbits $\pm z_H(\cdot, \mu)$ guarantied by Theorem 3.2. In particular, L^O is $\mathbb{Z}_2$-symmetric, i.e., $L^O = -L^O$.

Remark 3.8. *In Theorem 3.3(i),(iii), the attracting sets L and L^O, respectively, are also attractors in accordance with Ruells's definition using pseudo-orbits [35] and Milnor's definition using ω-limit sets [29]. In the case (ii), the attracting set L' is a Ruelle's attractor, but Milnor's attractor is simply the pair of the equilibrium points $\pm \boldsymbol{d}_0$ because these are the only ω-limit points of non-equilibrium trajectories in L'.*

Remark 3.9. *Consider system* (3.33) *with the parameter $\mu \in (\mu_\ell, \mu_r)$ and functions* (3.34). *Assume that $\sigma(\mu)$ strictly decreases and has a zero μ_o on the interval (μ_ℓ, μ_r), i.e., $\sigma(\mu_o) = 0$ as in Theorem 3.2. Let ρ, κ^*, κ_* be defined by* (3.38) *and* (3.39) *with $\alpha = \alpha(\mu_o)$, $\gamma = \gamma(\mu_o)$. Using part (iii) of Theorem 3.3 and the continuity argument, one can show that if either $\kappa^* < \kappa(\mu_o) < \kappa_*$ and $\rho > 0$ or $\kappa^* < \kappa(\mu_o) < 0$ and $-1 < \rho < 0$, then system* (3.33) *has an attracting periodic orbit $L^O(\mu)$, which depends continuously on μ on some interval $(\mu_o - \delta, \mu_o + \delta)$ and is given by* (3.44) *and* (3.45) *with $\Theta(\cdot,\cdot) = \Theta_{\mu_o}(\cdot,\cdot)$ for $\mu = \mu_o$, i.e., $L^O(\mu_o) = L^O$. Part of this orbit belongs to $\overline{S_0}$, the other part belongs to $\Omega_+ \cup \Omega_-$.*

4. Poincaré map

The proof of the above theorems is based on the analysis of the Poincaré map, which we define in this section. Due to relation (3.5), the boundary of the sliding region $S_0 \subset S$ is the union $\ell_- \cup \ell_+$ of the straight lines

$$\ell_- = \left\{ \boldsymbol{z} \in S : \boldsymbol{c}^T A \boldsymbol{z} = -1 \right\}, \qquad \ell_+ = \left\{ \boldsymbol{z} \in S : \boldsymbol{c}^T A \boldsymbol{z} = 1 \right\}. \tag{4.1}$$

On these lines, the vector fields $\Phi_\pm$ defined by (3.16) satisfy

$$\pm \boldsymbol{n}_S{}^T \Phi_\mp > 0 \ \text{ on } \ \ell_\pm, \qquad \Phi_\pm \cdot \boldsymbol{n}_S = 0 \ \text{ on } \ \ell_\pm \tag{4.2}$$

(cf. (3.21)). Moreover,

$$\Phi_\pm(\boldsymbol{z}) = A\boldsymbol{z} \pm \boldsymbol{b} = B\boldsymbol{z} \in S, \qquad \boldsymbol{z} \in \ell_- \cup \ell_+ \tag{4.3}$$

(cf. (3.23)). Relations (3.19) and (3.20) imply that if a trajectory either starts in, or enters, S_0, then it either remains in S_0 forever or continues within S_0 until it leaves the strip S_0 through its boundary into one of the half-spaces $\Omega_\pm$. Moreover, the set of exit points from the sliding region S_0 is either the union $\ell_-^{out} \cup \ell_+^{out}$ in case $\sigma \ge 0$ or the closure $\overline{\ell_-^{out} \cup \ell_+^{out}}$ of this union in case $\sigma < 0$, where ℓ_-^{out}, ℓ_+^{out} are the rays

$$\ell_-^{out} = \{-\boldsymbol{w}_0 + \psi \boldsymbol{w} : \psi < 0\} \subset \ell_-, \qquad \ell_+^{out} = \{\boldsymbol{w}_0 + \psi \boldsymbol{w} : \psi > 0\} \subset \ell_+ \tag{4.4}$$

with $\boldsymbol{w}$ given by (3.40) and $\boldsymbol{w}_0$ defined by

$$\langle \boldsymbol{c}, \boldsymbol{w}_0 \rangle = 0, \quad \langle \boldsymbol{c}, A\boldsymbol{w}_0 \rangle = 1, \quad \left\langle \boldsymbol{c}, A^2\boldsymbol{w}_0 \right\rangle = -\langle \boldsymbol{c}, A\boldsymbol{b} \rangle. \tag{4.5}$$

Due to (4.2), a trajectory that leaves S_0 through a point $\boldsymbol{p} \in \ell_-^{out} \cup \ell_+^{out}$ is tangent to the plane $S \supset S_0$ at $\boldsymbol{p}$.

We denote by $T^r(\psi)$ the *first return time to the switching plane* S from the set $\ell_-^{out} \cup \ell_+^{out} \subset \overline{S_0} \subset S$, i.e., $T^r(\psi) > 0$ is defined by

$$\Theta(T^r(\psi), \boldsymbol{z}') \in S_0; \;\; \Theta(t, \boldsymbol{z}') \notin S \;\; \text{for} \;\; t \in (0, T^r(\psi)); \;\; \boldsymbol{z}' = -\boldsymbol{w}_0 + \psi \boldsymbol{w}, \; \psi < 0; \tag{4.6}$$

$$\Theta(T^r(\psi), \boldsymbol{z}') \in S_0; \;\; \Theta(t, \boldsymbol{z}') \notin S \;\; \text{for} \;\; t \in (0, T^r(\psi)); \;\; \boldsymbol{z}' = \boldsymbol{w}_0 + \psi \boldsymbol{w}, \; \psi > 0. \tag{4.7}$$

By inspection, $T = T^r(\psi)$ is the least positive solution of the equation

$$F(\alpha, \gamma, \sigma, \psi, T) := \psi f(\alpha, \gamma, T) - \sigma g(\alpha, \gamma, T) = 0, \tag{4.8}$$

where f is defined by (3.36) and

$$\begin{aligned} g(\alpha, \gamma, T) := e^{-\alpha T} - \frac{1+\alpha^2}{1+(\alpha-\gamma)^2} e^{(\gamma-\alpha)T} \\ + \frac{(2\alpha-\gamma)\gamma}{1+(\alpha-\gamma)^2} \cos(T) - \frac{(\alpha^2-\alpha\gamma-1)\gamma}{1+(\alpha-\gamma)^2} \sin(T). \end{aligned} \tag{4.9}$$

Remark 4.1. *The function T^r can be discontinuous. For example, if $\alpha = -\gamma = 0.125$, then the function f given by Eq* (3.37) *has two roots $\pi < T_1 < T_2 < 2\pi$ and no roots on the set $(0, \pi] \cup [2\pi, 3\pi]$. Moreover, the function g given by* (4.9) *is strictly negative on the interval $T \in (0, 3\pi]$ (see Figure 2a). Therefore, if $\sigma = -1$, then $T^r(\psi) \notin [2\pi, 3\pi]$ for $\psi \geq 0$ and $T^r(0) > 3\pi$. On the other hand, if $\sigma = -1$, then the function $F(\alpha, \gamma, \sigma, \psi^*, \cdot)$ has two roots on the interval $[6, 7]$ for $\psi^* = 0.25$ (see Figure 2b), hence $T^r(\psi^*) \in [0, 7]$. Thus, $T^r([0, \psi^*])$ is a disconnected set, consequently T^r is discontinuous.*

We will use the Poincaré map

$$P : \{z = \text{sign}(\psi)\boldsymbol{w}_0 + \psi \boldsymbol{w} \in \ell_+^{out} \cup \ell_-^{out} : \psi \in (-\delta, 0) \cup (0, \delta)\} \to \ell_+^{out} \cup \ell_-^{out} \tag{4.10}$$

defined by

$$P(\boldsymbol{w}_0 + \psi \boldsymbol{w}) = \Theta(T^e(\psi), \boldsymbol{w}_0 + \psi \boldsymbol{w}) \in \ell_+^{out} \cup \ell_-^{out}, \qquad \psi \in (0, \delta), \tag{4.11}$$

$$T^e(\psi) \geq T^r(\psi), \tag{4.12}$$

$$\Theta(t, \boldsymbol{w}_0 + \psi \boldsymbol{w}) \in S_0, \quad t \in \left[T^r(\psi), T^e(\psi)\right), \tag{4.13}$$

on a part of the ray ℓ_+^{out}, and by

$$P(-\boldsymbol{w}_0 + \psi \boldsymbol{w}) = -P(\boldsymbol{w}_0 - \psi \boldsymbol{w}), \qquad \psi \in (-\delta, 0), \tag{4.14}$$

on a part of the ray ℓ_-^{out}. Here T^e is the first return time to the part $\ell_+^{out} \cup \ell_-^{out}$ of the boundary of S_0. The domain of the Poincaré map will be discussed in the proofs.

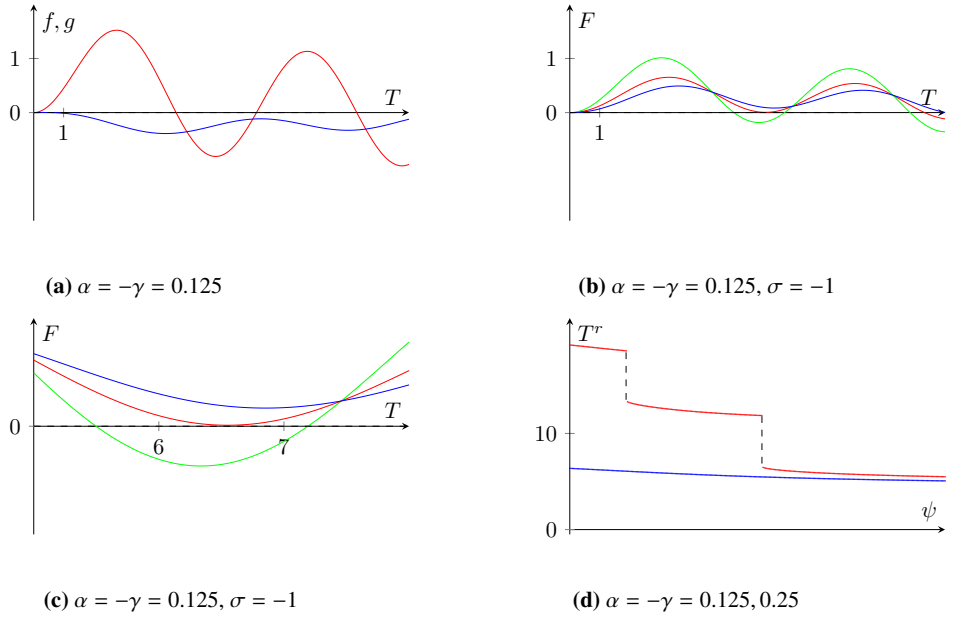

(a) $\alpha = -\gamma = 0.125$

(b) $\alpha = -\gamma = 0.125$, $\sigma = -1$

(c) $\alpha = -\gamma = 0.125$, $\sigma = -1$

(d) $\alpha = -\gamma = 0.125, 0.25$

Figure 2. (a) The graph of the functions $f(\alpha, \gamma, T)$ (red) and $g(\alpha, \gamma, T)$ (blue) for the parameters $\alpha = 0.125 = -\gamma$ (cf. (3.37), (4.9)). (b) The graph of $F(\alpha, \gamma, \sigma, \psi, T)$ with $\alpha = -\gamma = 0.125$, $\sigma = -1$ for $\psi = 0.5$ (green), $\psi = 0.25$ (red) and $\psi = 0.125$ (blue) (cf. (4.8)). The least positive root is T^r. (c) A zoomed-in view of the interval $[5, 8]$ from Figure 2b. (d) The graph of the first return time $T^r(\psi)$ for two sets of parameter values: $\alpha = 0.125 = -\gamma$ and $\sigma = -1$ (red); $\alpha = 0.25 = -\gamma$ and $\sigma = -1$ (blue).

Equivalently, by identifying the ray $\ell_+^{out} \ni \boldsymbol{w}_0 + \psi \boldsymbol{w}$ with the positive semiaxis $\mathbb{R}_+ \ni \psi$ and the ray $\ell_-^{out} \ni -\boldsymbol{w}_0 + \psi \boldsymbol{w}$ with the negative semiaxis $-\mathbb{R} \ni \psi$, the Poincaré map can be interpreted as the scalar function $P^c : (-\delta, 0) \cup (0, \delta) \to \mathbb{R}$ given either by

$$P(\operatorname{sign}(\psi)\boldsymbol{w}_0 + \psi \boldsymbol{w}) = \operatorname{sign}(\psi)\boldsymbol{w}_0 + P^c(\psi)\,\boldsymbol{w}, \qquad \psi P^c(\psi) \geq 0, \tag{4.15}$$

or by

$$P(\operatorname{sign}(\psi)\boldsymbol{w}_0 + \psi \boldsymbol{w}) = -\operatorname{sign}(\psi)\boldsymbol{w}_0 + P^c(\psi)\,\boldsymbol{w}, \qquad \psi P^c(\psi) \leq 0. \tag{4.16}$$

Slightly abusing the terminology, the function P^c will be also called the Poincaré map whenever this does not lead to confusion.

Remark 4.2. *By definition, a fixed point ψ_* of the function P^c given by* (4.15) *defines two different periodic orbits $\pm\Theta(t, \boldsymbol{w}_0 + \psi_* \boldsymbol{w}) = \pm\Theta(t + p, \boldsymbol{w}_0 + \psi_* \boldsymbol{w})$, $t \in \mathbb{R}$, of system* (3.1) *of an a priori unknown period $p > 0$. On the other hand, a fixed point ψ_* of the function P^c given by* (4.16) *defines a $\mathbb{Z}_2$-symmetric periodic orbit, i.e., an antiperiodic orbit satisfying $\Theta(t + p/2, \boldsymbol{w}_0 + \psi_* \boldsymbol{w}) = -\Theta(t, \boldsymbol{w}_0 + \psi_* \boldsymbol{w})$, $t \in \mathbb{R}$. The proof of the theorems presented in Sections 3.4 and 3.5 involves the construction of an interval, where P^c satisfies the conditions of the intermediate value theorem. It is important to note that discontinuities of the first return time T^r to the plane S induce discontinuities of the Poincaré map.*

5. Numerical examples

Figure 2 demonstrates that the function T^r, the first return time to the switching plane S from the set $\ell_+^{out} \cup \ell_-^{out}$, is discontinuous for specific parameters α and γ (cf. Remark 4.1). Figure 2a shows that $g(\alpha, \gamma, T) < 0$ for $T \in (0, 10]$ and $f(\alpha, \gamma, T) < 0$ for $T \in (0, 4] \cup [8, 10]$. According to Figure 2b, the function $F(\alpha, \gamma, \sigma, \psi, T)$ with $\alpha = -\gamma = 0.125$ and $\sigma = -1$ has two roots in the interval $[4, 8]$ for $\psi = 0.5$ (green curve) and no roots in the same interval when either $\psi = 0.25$ (red curve) or $\psi = 0.125$ (blue curve). Hence, for $\alpha = -\gamma = 0.125$ and $\sigma = -1$, the least positive root $T = T^r(\psi)$ of $F(\alpha, \gamma, \sigma, \psi, T) = 0$ has a jump between $\psi = 0.25$ and $\psi = 0.5$, which is shown in Figure 2d (red curve). On the other hand, the function T^r is continuous on the interval $[0, 0.5]$ for $\alpha = -\gamma = 0.25$ and $\sigma = -1$ (the blue curve in Figure 2d). Figure 3a presents the corresponding continuous Poincaré map P^c. The intersection of the graph of P^c with the bisector (dashed line) ensures that system (3.1) has two periodic orbits in agreement with Theorem 3.2 (see also Remark 3.5). Figure 3b shows that for $\alpha = -\gamma = 0.125$ and $\sigma = 0.25$, the Poincaré map P^c given by (4.15) has discontinuities, which correspond to the discontinuities of T^r shown in Figure 2d. However, the equation $\psi = P^c(\psi)$ has a solution, which is a continuity point of P^c (shown as the intersection of the red curve with the dashed bisector), proving the existence of two periodic orbits (cf. Remark 4.2).

Figure 4a presents the graphs of the Poincaré map (4.16) for $\kappa = -0.25$ (blue curve) and $\kappa = 0$ (red curve) (the other parameters are $\alpha = -\gamma = 0.125$, $\sigma = 0$; for these parameters, $\rho > 0$, cf. (3.38)). The intersection of the blue curve with the bisector (dashed line) proves the existence of the periodic orbit L^O in agreement with part (iii) of Theorem 3.3. Figure 4b demonstrates the robustness of this $\mathbb{Z}_2$-symmetric periodic orbit with respect to variations of the parameter σ in accordance with Remark 3.9. There is no periodic orbit for $\kappa = 0$.

Figures 5 and 6 show the scatter plot of points $\Theta(t, z')$ for $t = 40$ and

$$z' \in G = \{0.25(k_1, k_2, k_3) : k_i \in \mathbb{Z}, -6 \le k_i \le 6,\ i = 1, 2, 3\}.$$

In Figure 5, where $\alpha = 0.125 = -\gamma$ and $\kappa = 1$, the attracting set is the segment of equilibrium states L for $\sigma = 0$ (Figure 5a) and the union of two periodic orbits $L^H(\sigma)$ and $-L^H(\sigma)$ for $\sigma = -0.125$ (Figure 5b). According Theorem 3.2, the periodic orbits bifurcate from the end points of L as the bifurcation parameter $\mu = \sigma$ becomes negative. Figure 5c, where Figure 5a,5b is overlapped, confirms that the periodic orbits $\pm L^H(\sigma)$ are close to the end points of equilibrium set L.

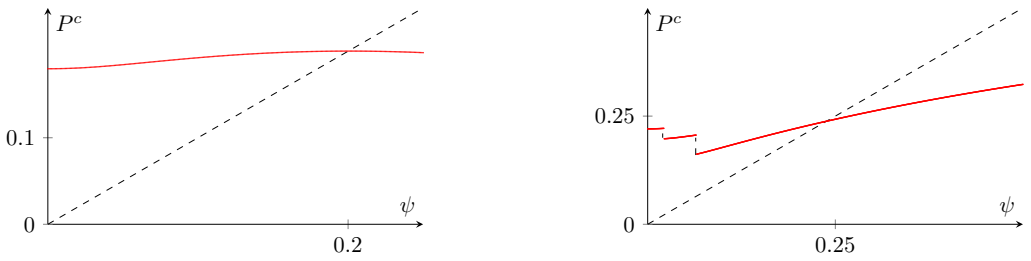

(a) $\alpha = -\gamma = 0.125$ **(b)** $\alpha = -\gamma = 0.25$

Figure 3. The graph of the Poincaré map P^c given by (4.15) for two parameter sets. On both panels, $\sigma = -0.25$, $\kappa = 1$. The dashed line represents the bisector.

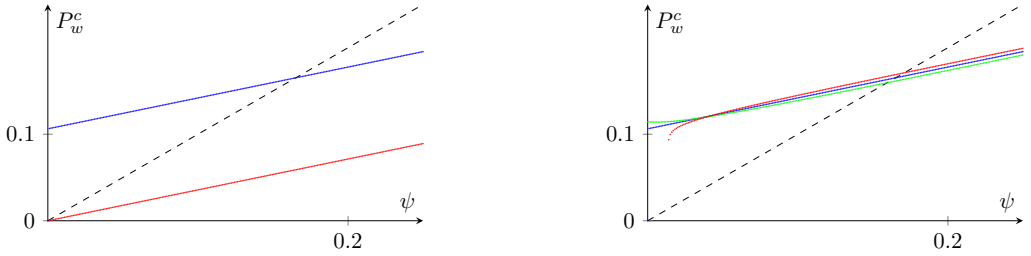

(a) $\kappa = 0, -0.25$ **(b)** $\sigma = 0, \pm 0.0025$

Figure 4. (a) The graph of the Poincaré map P^c given by (4.16) for $\kappa = 0$ (red) and $\kappa = -0.25$ (blue); the other parameters are $\alpha = -\gamma = 0.25$, $\sigma = 0$. (b) The graph of P^c for the parameters $\alpha = -\gamma = 0.25$, $\kappa = -0.25$ and $\sigma = 0$ (blue); $\sigma = 0.0025$ (green); $\sigma = -0.0025$ (red).

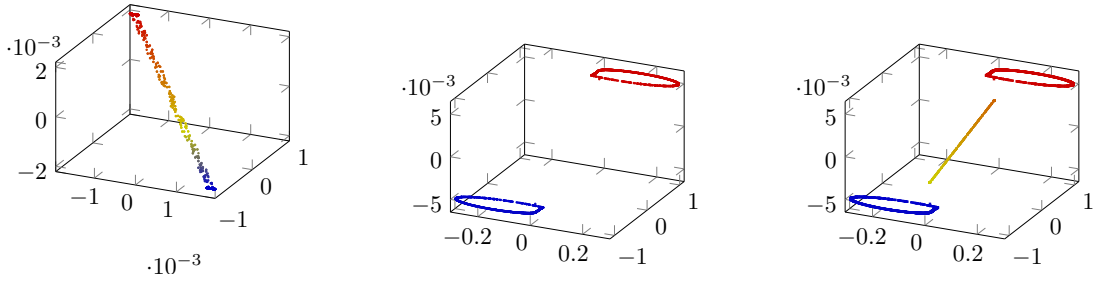

(a) **(b)** **(c)**

Figure 5. The scatter plot of points $\Theta(t, z')$ with $t = 40$, $z' \in G$ for $\alpha = -\gamma = 0.125$, $\kappa = 1$ and (a) $\sigma = 0$; (b) $\sigma = -0.125$. (c) Combined panels (a) and (b).

Figure 6, where $\alpha = 0.25 = -\gamma$, $\kappa = -1$, shows the points from G converging to the periodic orbit $L^O(\sigma)$ for $\sigma = 0$ and $\sigma = -0.125$ in agreement with Remark 3.9.

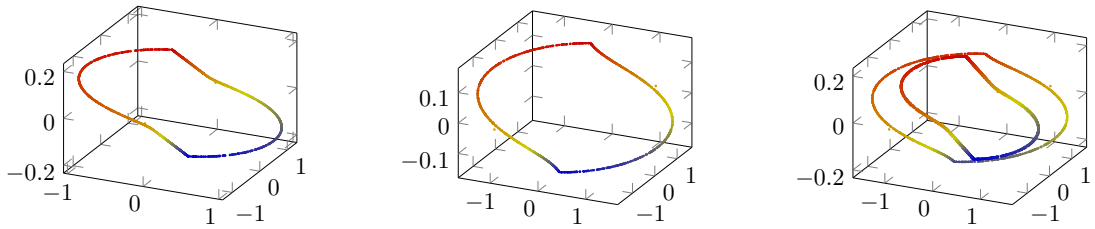

(a) **(b)** **(c)**

Figure 6. The scatter plot of points $\Theta(t, z')$ with $t = 40$, $z' \in G$ for $\alpha = -\gamma = 0.25$, $\kappa = -1$ and (a) $\sigma = 0$; (b) $\sigma = -0.125$. (c) Combined panels (a) and (b).

In Figure 7, where $\alpha = 0.125 = -\gamma$ and $\kappa = -2$, points from G converge to the periodic orbit L^O for $\sigma = 0$ in agreement with part (iii) of Theorem 3.3 (Figure 7a). For $\sigma = -0.125$, the periodic orbit $L^O(\sigma)$ coexists with the small periodic orbits $\pm L^H(\sigma)$ (Figure 7b). Moreover, part of G belongs to the basin of attraction of $L^O(\sigma)$, while another part of G belongs to the basin of attraction of $\pm L^H(\sigma)$. Figure 7c, where Figure 7a,7b is overlapped, illustrates the continuous transformation of the periodic orbit $L^O(\sigma)$ as the parameter σ is varied from $\sigma = 0$ to $\sigma = -0.125$.

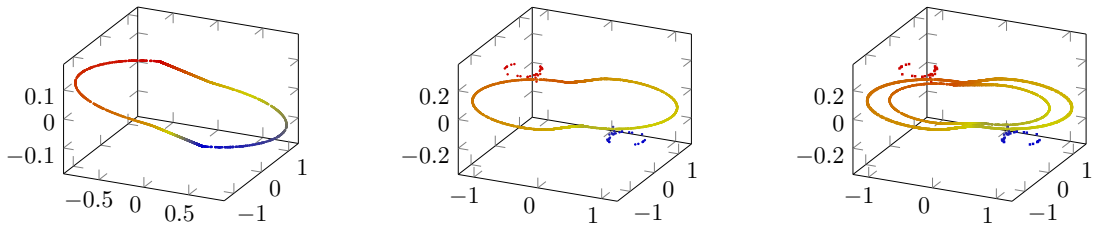

(a) (b) (c)

Figure 7. The scatter plot of points $\Theta(t, z')$ with $t = 40$, $z' \in G$ for $\alpha = -\gamma = 0.125$, $\kappa = -2$ and (a) $\sigma = 0$; (b) $\sigma = -0.125$. (c) Combined panels (a) and (b).

6. Conclusions

We analyzed stick-slip dynamics of the 3D Lur'e system with the sign nonlinearity and an example of a controlled 1.5-degrees of freedom system with a strongly nonlinear frictional interface assuming the Coulomb friction combined with the Stribeck effect. The latter is approximated by a negative viscous damping. We showed a bifurcation of periodic orbits from the equilibrium set and the existence of periodic (and non-periodic) attractors. This is in agreement with other results showing that the velocity-weakening (Stribeck) effect can be the primary cause of instability, persistent stick-slip oscillations and the so-called hunting phenomenon in PID controlled systems (see, e.g., [9]).

The low-dimensionality of the system plays an important role for the above analysis because the switching surface has dimension two and the Poincaré map is one-dimensional. It would be interesting and more challenging to consider higher-dimensional Lur'e systems, which are however beyond the scope of this paper. In particular, one would hope that dynamics of the two-dimensional Poincaré map associated with the 2-degrees of freedom feedback system with a frictional interface could be still tractable.

As shown by extensive experimental studies (see e.g., [10, 19, 22]), both adhesion-stiction and continuous sliding mechanisms are essential for modeling a frictional interface between moving bodies [3, 5] and dynamic transitions in the friction processes, from the attachment-detachment cycles [45] to the stick-slip motion and continuous sliding [38]. Multiple empirical and heuristic approaches capturing the so-called presliding phase of the kinetic friction include the Dahl model [12], the Maxwell-slip model [23], the LuGre model [13], generic model at asperity level [2], two-state dynamic friction model with elastoplasticity [32]. Moreover, sophisticated models of the frictional interaction of contact surfaces from nano- to the meso-scale are available [42]. However, a transition to lumped parameter modeling of inertial pairs with frictional interfaces is non-trivial. As such, the Amonton-Coulomb dry friction law is based on several strong simplifying assumptions: (i) no viscous friction effects at the interface are included; (ii) the breakaway static friction force due to adhesion, with the associated Stribeck effect at the transients between the presliding and gross sliding regimes, is not accounted for; (iii) the so-called smooth sliding with the averaged constant Coulomb friction force is assumed, hence true stick-slip dynamics at the atomic level with the related Frenkel-Kontorowa and Prandtl-Tomlinson type interactions [30, 39] are not addressed. Furthermore, smooth breakaway frictional force transitions, which are characteristic of the presliding regime at the start of motion [3], are disregarded. Still, incorporating the Coulomb friction discontinuity in the equations of motion is considered a crucial step for modeling, stability analysis and control design of mechanical

systems [1, 36]. Moreover, the inclusion of the Stribeck effect, which is essential for lubricated kinetic friction in a lower range of relative velocities, is relevant, especially for analysis of stability and convergence of the motion state trajectories. Dynamics with more complex friction transitions in presliding phase have been studied, for example, in [33].

Use of Generative-AI tools declaration

The authors declare they have not used Artificial Intelligence (AI) tools in the creation of this article.

Conflict of interest

The authors declare no conflicts of interest.

References

1. S. Adly, H. Attouch, A. Cabot, Finite time stabilization of nonlinear oscillators subject to dry friction, In: P. Alart, O. Maisonneuve, R. T. Rockafellar, *Nonsmooth mechanics and analysis*, Advances in Mechanics and Mathematics, Springer, Boston, **12** (2006), 289–304. https://doi.org/10.1007/0-387-29195-4_24
2. F. Al-Bender, V. Lampaert, J. Swevers, A novel generic model at asperity level for dry friction force dynamics, *Tribol. Lett.*, **16** (2004), 81–93. https://doi.org/10.1023/B:TRIL.0000009718.60501.74
3. F. Al-Bender, J. Swevers, Characterization of friction force dynamics, *IEEE Contr. Syst. Mag.*, **28** (2008), 64–81. https://doi.org/10.1109/MCS.2008.929279
4. A. A. Andronov, S. E. Khaikin, A. A. Vitt, *Theory of oscillators*, Elsevier, 1966. https://doi.org/10.1016/C2013-0-06631-5
5. B. Armstrong-Hélouvry, P. Dupont, C. C. De Wit, A survey of models, analysis tools and compensation methods for the control of machines with friction, *Automatica*, **30** (1994), 1083–1138. https://doi.org/10.1016/0005-1098(94)90209-7
6. V. Avrutin, L. Gardini, I. Sushko, F. Tramontana, *Continuous and discontinuous piecewise-smooth one-dimensional maps: invariant sets and bifurcation structures*, World Scientific, 2019.
7. M. D. Bernardo, C. J. Budd, A. R. Champneys, P. Kowalczyk, A. B. Nordmark, G. O. Tost, et al., Bifurcations in nonsmooth dynamical systems, *SIAM Rev.*, **50** (2008), 629–701. https://doi.org/10.1137/050625060
8. J. J. B. Biemond, N. van de Wouw, H. Nijmeijer, Bifurcations of equilibrium sets in mechanical systems with dry friction, *Phys. D*, **241** (2012), 1882–1894. https://doi.org/10.1016/j.physd.2011.05.006
9. A. Bisoffi, R. Beerens, W. Heemels, H. Nijmeijer, N. van de Wouw, L. Zaccarian, To stick or to slip: a reset PID control perspective on positioning systems with friction, *Annu. Rev. Control*, **49** (2020), 37–63. https://doi.org/10.1016/j.arcontrol.2020.04.010
10. F. P. Bowden, D. Tabor, *The friction and lubrication of solids*, Vol. 1, Oxford Academic, 2001. https://doi.org/10.1093/oso/9780198507772.001.0001

11. F. M. Callier, C. A. Desoer, *Linear system theory*, Springer, 1991. https://doi.org/10.1007/978-1-4612-0957-7

12. P. R. Dahl, *A solid friction model*, SAMSO Technical Report, The Aerospace Corporation, El Segundo, 1968.

13. C. C. De Wit, H. Olsson, K. J. Aström, P. Lischinsky, A new model for control of systems with friction, *IEEE Trans. Automat. Contr.*, **40** (1995), 419–425. https://doi.org/10.1109/9.376053

14. M. di Bernardo, C. Budd, A. R. Champneys, P. Kowalczyk, *Piecewise-smooth dynamical systems: theory and applications*, Applied Mathematical Sciences,Vol. 163, Springer Science & Business Media, 2008. https://doi.org/10.1007/978-1-84628-708-4

15. M. I. Feigin, Doubling of the oscillation period with C-bifurcations in piecewise-continuous systems, *J. Appl. Math. Mech.*, **34** (1970), 836–843. https://doi.org/10.1016/0021-8928(70)90066-3

16. A. F. Filippov, *Differential equations with discontinuous righthand sides*, Mathematics and its Applications, Vol. 18, Springer Dordrecht, 1988. https://doi.org/10.1007/978-94-015-7793-9

17. P. Flores, J. Ambrósio, H. M. Lankarani, Contact-impact events with friction in multibody dynamics: back to basics, *Mech. Mach. Theory*, **184** (2023), 105305. https://doi.org/10.1016/j.mechmachtheory.2023.105305

18. O. V. Gendelman, Bifurcations of nonlinear normal modes of linear oscillator with strongly nonlinear damped attachment, *Nonlinear Dyn.*, **37** (2004), 115–128. https://doi.org/10.1023/B:NODY.0000042911.49430.25

19. T. Koizumi, H. Shibazaki, A study of the relationships governing starting rolling friction, *Wear*, **93** (1984), 281–290. https://doi.org/10.1016/0043-1648(84)90202-3

20. P. Kowalczyk, M. di Bernardo, A. R. Champneys, S. J. Hogan, M. Homer, P. T. Piiroinen, et al., Two-parameter discontinuity-induced bifurcations of limit cycles: classification and open problems, *Int. J. Bifurcat. Chaos*, **16** (2006), 601–629. https://doi.org/10.1142/S0218127406015015

21. M. Kunze, *Non-smooth dynamical systems*, Lecture Notes in Mathematics, Vol. 1744, Springer Berlin, Heidelberg, 2000. https://doi.org/10.1007/BFb0103843

22. V. Lampaert, F. Al-Bender, J. Swevers, Experimental characterization of dry friction at low velocities on a developed tribometer setup for macroscopic measurements, *Tribol. Lett.*, **16** (2004), 95–105. https://doi.org/10.1023/B:TRIL.0000009719.53083.9e

23. B. J. Lazan, *Damping of materials and members in structural mechanics*, 1 Ed., Vol. 214, Pergamon Press, 1968.

24. R. I. Leine, D. H. V. Campen, A. D. Kraker, L. V. D. Steen, Stick-slip vibrations induced by alternate friction models, *Nonlinear Dyn.*, **16** (1998), 41–54. https://doi.org/10.1023/A:1008289604683

25. R. I. Leine, H. Nijmeijer, *Dynamics and bifurcations of non-smooth mechanical systems*, Springer Science & Business Media, 2013.

26. J. Llibre, E. Ponce, J. Ros, F. Torres, On the fold-Hopf bifurcation for continuous piecewise linear differential systems with symmetry, *Chaos*, **20** (2010), 033119. https://doi.org/10.1063/1.3486073

27. O. Makarenkov, J. S. W. Lamb, Dynamics and bifurcations of nonsmooth systems: a survey, *Phys. D*, **241** (2012), 1826–1844. https://doi.org/10.1016/j.physd.2012.08.002

28. A. Marigo, A. Bicchi, Rolling bodies with regular surface: controllability theory and applications, *IEEE Trans. Automat. Control*, **45** (2000), 1586–1599. https://doi.org/10.1109/9.880610

29. J. Milnor, On the concept of attractor, *Commun. Math. Phys.*, **99** (1985), 177–195. https://doi.org/10.1007/BF01212280

30. V. Popov, J. Gray, Prandtl-Tomlinson model: history and applications in friction, plasticity, and nanotechnologies, *J. Appl. Math. Mech.*, **92** (2012), 683–708. https://doi.org/10.1002/zamm.201200097

31. M. Posa, M. Tobenkin, R. Tedrake. Stability analysis and control of rigid-body systems with impacts and friction, *IEEE Trans. Automat. Control*, **61** (2016), 1423–1437. https://doi.org/10.1109/TAC.2015.2459151

32. M. Ruderman, T. Bertram, Two-state dynamic friction model with elasto-plasticity, *Mech. Syst. Signal Process.*, **39** (2013), 316–332. https://doi.org/10.1016/j.ymssp.2013.03.010

33. M. Ruderman, D. Rachinskii, Use of Prandtl-Ishlinskii hysteresis operators for Coulomb friction modeling with presliding, *J. Phys.: Conf. Ser.*, **811** (2017), 012013. https://doi.org/10.1088/1742-6596/811/1/012013

34. M. Ruderman, A. Zagvozdkin, D. Rachinskii, Dynamics of inertial pair coupled via frictional interface, *2022 IEEE 61st Conference on Decision and Control (CDC)*, 2023, 1324–1329. https://doi.org/10.1109/CDC51059.2022.9993163

35. D. Ruelle, Small random perturbations of dynamical systems and the definition of attractors, *Commun. Math. Phys.*, **82** (1981), 137–151. https://doi.org/10.1007/BF01206949

36. S. W. Shaw, On the dynamic response of a system with dry friction, *J. Sound Vib.*, **108** (1986), 305–325. https://doi.org/10.1016/S0022-460X(86)80058-X

37. D. J. W. Simpson, *Bifurcations in piecewise-smooth continuous systems*, Vol. 70, World Scientific, 2010. https://doi.org/10.1142/7612

38. A. Socoliuc, R. Bennewitz, E. Gnecco, E. Meyer, Transition from stick-slip to continuous sliding in atomic friction: entering a new regime of ultralow friction, *Phys. Rev. Lett.*, **92** (2004), 134301. https://doi.org/10.1103/PhysRevLett.92.134301

39. M. Urbakh, J. Klafter, D. Gourdon, J. Israelachvili, The nonlinear nature of friction, *Nature*, **430** (2004), 525–528. https://doi.org/10.1038/nature02750

40. V. I. Utkin, *Sliding modes in control optimization*, Communications and Control Engineering, Springer Berlin, Heidelberg, 1992. https://doi.org/10.1007/978-3-642-84379-2

41. A. F. Vakakis, O. V. Gendelman, L. A. Bergman, D. M. McFarland, G. Kerschen, Y. S. Lee, *Nonlinear targeted energy transfer in mechanical and structural systems*, Solid Mechanics and Its Applications, Vol. 156, Springer Dordrecht, 2009. https://doi.org/10.1007/978-1-4020-9130-8

42. A. Vanossi, N. Manini, M. Urbakh, S. Zapperi, E. Tosatti, Colloquium: modeling friction: from nanoscale to mesoscale, *Rev. Mod. Phys.*, **85** (2013), 529. https://doi.org/10.1103/RevModPhys.85.529

43. S. Wu, G. Bercu, Padé approximants for inverse trigonometric functions and their applications, *J. Inequal. Appl.*, **2017** (2017), 31. https://doi.org/10.1186/s13660-017-1310-6

44. V. A. Yakubovich, G. A. Leonov, A. K. Gelig, *Stability of stationary sets in control systems with discontinuous nonlinearities*, Vol. 14, World Scientific, 2004. https://doi.org/10.1142/5442

45. H. Zeng, M. Tirrell, J. Israelachvili, Limit cycles in dynamic adhesion and friction processes: a discussion, *J. Adhesion*, **82** (2006), 933–943. https://doi.org/10.1080/00218460600875979

Appendix

A. Proof of Theorem 3.1

The following lemma establishes the equilibrium set of system (3.1) for each case considered in Theorem 3.1.

Lemma A.1. (a) *The origin is an equilibrium state of system* (3.1) *for all* σ.

(b) *The points* z_*^ξ *for* $\xi \in (-1, 1)$ *are equilibrium states iff* $\sigma = 0$.

(c) *The points* $\pm A^{-1}\boldsymbol{b}$ *are equilibrium states iff* $\sigma \leq 0$.

(d) *There are no other equilibrium states.*

Proof. From $0 \in S_0$, it follows that zero is an equilibrium, which proves (a). By inspection, the zeroes of the velocity fields $\Phi_\pm$ are given by $\mp A^{-1}\boldsymbol{b}$. The definition of $\Omega_\pm$ implies that $\mp A^{-1}\boldsymbol{b} \in \Omega_\pm$ iff $\boldsymbol{c}^T A^{-1}\boldsymbol{b} = \sigma < 0$, which proves (c) except for the case $\sigma = 0$. By (3.18), $z_*^\xi = -\xi A^{-1}\boldsymbol{b} \in \overline{S_0}$ iff $\sigma = 0$ and $|\xi| \leq 1$. Since the vector $A^{-1}\boldsymbol{b}$ belongs to the kernel of the matrix B, which according to (3.24) has rank 2, it follows that $z_*^\xi \in \overline{S_0}$ are equilibrium points, which proves (b) and completes the proof of (c) for the case $\sigma = 0$. Due to (3.19), there are no equilibrium points in $S_\pm$, which proves (d). □

Due to conditions (3.4) and (3.5), there is an open domain $\mathcal{U} \subset \mathbb{R}^3$ and a bounded function $T_1 : \mathcal{U} \to \mathbb{R}_+$ such that $\Theta(T_1(z'), z') \in \overline{S_0}$ for $z' \in \mathcal{U}$ and $\mathcal{U}$ contains all the equilibrium states that belong to S_0. Therefore, using the continuity of the flow and the fact that (linear) dynamics in S_0 is given by (3.22), all the stability properties listed in Theorem 3.1 for the equilibrium states that belong to S_0 (i.e., for z_*^0 and z_*^ξ with $|\xi| < 1$ in the case $\sigma = 0$) follow from the stability properties of the matrix $B|_S$ (cf. (3.25) and (3.26)). By the same token, the instability of the equilibrium states $z_*^{\pm 1} = \pm\boldsymbol{d}_0 \in \overline{S_0}$ in the case $\sigma = 0$, $\kappa \leq 0$ follows from the fact that the repeated zero eigenvalue of $B|_S$ has geometric multiplicity one; and, the instability of the states $z_*^\pm = \pm\boldsymbol{d}_0 \in \Omega_\pm$ in the case $\sigma < 0$ follows from the instability of the matrix A.

It remains to show that if $\sigma = 0$, $\kappa > 0$, then the equilibrium states $\pm\boldsymbol{d}_0$ are stable and the equilibrium set L given by (3.31) is attracting. The relations $\sigma = 0$, $\kappa > 0$ imply that the flow in S_0 is parallel to the vector $\boldsymbol{v}_2 = A\boldsymbol{w}$ (cf. (3.27) and (3.29)) and directed towards the straight line $\{\xi\boldsymbol{d}_0 : \xi \in \mathbb{R}\}$, which contains the equilibrium set L. Therefore, for any z' sufficiently close to L, the trajectory $\Theta(t, z')$ either converges to an equilibrium state or reaches the part $\ell_-^{out} \cup \ell_+^{out}$ of the boundary of S_0 at a time $t \geq T_1(z')$. More precisely, the relations $\sigma = 0$, $\kappa > 0$ imply that $\{\boldsymbol{d}_0, A\boldsymbol{w}\}$ (where $\boldsymbol{w}$ is a direction vector of $\ell_\pm$) is a basis in S and, based on the decomposition $\Theta(T_1(z'), z') = \xi(z')\boldsymbol{d}_0 + \eta(z')A\boldsymbol{w}$, if $|\xi(z')| \leq 1$, then $\Theta(t, z') \to \xi(z')\boldsymbol{d}_0 \in L$, while if $|\xi(z')| > 1$, then $z = \Theta(t, z') \in \ell_-^{out} \cup \ell_+^{out}$ for some $t \geq T_1(z')$. In

the latter case, the trajectory continues from the point $z = \boldsymbol{d}_0 + \psi \boldsymbol{w} \in \ell_+^{out}$ with a sufficiently small $\psi > 0$ (resp., $z = -\boldsymbol{d}_0 + \psi \boldsymbol{w} \in \ell_-^{out}$ with $\psi < 0$) to the point $\Theta(T^r, z) = \boldsymbol{d}_0 + \psi e^{T^r A}\boldsymbol{w} \in \overline{S_0}$ (resp., $\Theta(T^r, z) = -\boldsymbol{d}_0 + \psi e^{T^r A}\boldsymbol{w} \in \overline{S_0}$), where $T^r > 0$ is the least positive root of function (3.37), i.e.,

$$e^{(\gamma-\alpha)T^r} - \cos(T^r) + (\alpha - \gamma)\sin(T^r) = 0. \tag{A.1}$$

Again, using the decomposition $e^{T_r A}\boldsymbol{w} = \xi_w \boldsymbol{d}_0 + \eta_w A\boldsymbol{w}$, we see that if $\xi_w \le 0$, then the trajectory $\Theta(t, \pm\boldsymbol{d}_0 + \psi e^{T_r A}\boldsymbol{w})$ converges along S_0 to the equilibrium state $(\pm 1 + \psi\xi_w)\boldsymbol{d}_0$; alternatively, if $\xi_w > 0$, then the trajectory reaches $\ell_+^{out} \cup \ell_-^{out}$, i.e., the Poincaré map is well-defined by (4.10)–(4.15). Moreover, due to $\sigma = 0$, this map is simply linear, $P_c(\psi) = \rho\psi$, and the coefficient $\rho > 0$ is defined by the decomposition

$$e^{T^r A}\boldsymbol{w} = \rho\, \boldsymbol{w} + \chi A\boldsymbol{w} \tag{A.2}$$

along the basis $\{\boldsymbol{w}, A\boldsymbol{w}\}$ in S. Now, using the decomposition $\boldsymbol{w} = \boldsymbol{u} + \boldsymbol{v}$, where $\boldsymbol{u}$ belongs to the invariant subspace of A corresponding to the eigenvalues $\alpha \pm i$ and $\boldsymbol{v}$ is an eigenvector of A corresponding to the eigenvalue γ, one obtains

$$e^{T^r A}\boldsymbol{w} = e^{\alpha T^r}(\cos(T^r) - \alpha\sin(T^r))\boldsymbol{u} + e^{\alpha T^r}\sin(T^r)A\boldsymbol{u} + e^{\gamma T^r}\boldsymbol{v}. \tag{A.3}$$

Combining (A.2), (A.3) and $A\boldsymbol{v} = \gamma\boldsymbol{v}$ gives

$$\rho = e^{\alpha T^r}(\cos(T^r) - \alpha\sin(T^r)) = e^{\gamma T^r}(1 - \gamma e^{(\alpha-\gamma)T^r}\sin(T^r)), \tag{A.4}$$

$$\chi = e^{\alpha T^r}\sin(T^r), \tag{A.5}$$

which agrees with (3.38) and (A.1). By inspection, the least positive root of (A.1) satisfies $T^r \in (\pi, 2\pi)$, hence (A.4) implies

$$\rho \le e^{\gamma T^r} < 1 \tag{A.6}$$

due to $\gamma < 0$. Since $\rho < 1$, the iterations of the Poincaré map P^c converge to zero, which completes the proof.

B. Proof of Theorem 3.2

We begin with three auxiliary lemmas and an auxiliary theorem.

Lemma B.2. *Let $\alpha \ge 1$, $\gamma < 0$. Then,*

$$-\frac{1}{\gamma}\ln\left(1 - \frac{(2\alpha - \gamma)\gamma}{(1 + (\alpha - \gamma)^2)\alpha^2}\right) < \arctan\left(\frac{2\alpha - \gamma}{\alpha^2 - \alpha\gamma - 1}\right). \tag{B.1}$$

Proof. Due to the Shafer–Fink inequality [43]

$$\arctan(x) > \frac{3x}{1 + 2\sqrt{1 + x^2}}, \qquad x > 0,$$

and the inequalities

$$\ln(1 + x) < x; \quad x > 0; \qquad \frac{3x}{1 + 2\sqrt{1 + x^2}} > \frac{3x}{1 + 3x}, \quad x \ge 1,$$

it suffices to show that

$$\frac{2\alpha-\gamma}{(1+(\alpha-\gamma)^2)\alpha^2} < \frac{3(2\alpha-\gamma)}{\alpha^2-\alpha\gamma-1+3(2\alpha-\gamma)},$$

which is equivalent to

$$3\alpha^2(\alpha-\gamma)^2+2\alpha^2+\alpha\gamma+1-3(2\alpha-\gamma)>0.$$

Rearranging,

$$3(\alpha-\gamma)(\alpha^3-1)-\alpha\gamma(3(\alpha-\gamma)\alpha-1)+(2\alpha-1)(\alpha-1)>0,$$

which holds true in the domain $\alpha \geq 1$, $\gamma < 0$. □

Let us consider functions (3.37) and (4.9).

Lemma B.3. *Let $\alpha > 0$, $\gamma < 0$. Then,*

(a) $f(\alpha,\gamma,t) = \frac{1}{2}\left(1+(\gamma-\alpha)^2\right)t^2 + O(t^3)$ *as* $t \to 0$;
(b) $f(\alpha,\gamma,t) > 0$ *for* $t \in (0, t_1+\pi]$, *where*

$$t_1 := \frac{\pi}{2} - \arctan(\alpha-\gamma) \in (0,\pi/2); \tag{B.2}$$

(c) $f(\alpha,\gamma,t) < 0$ *for* $t \in [2t_1+\pi, 2\pi]$ *and*

$$\frac{\partial f}{\partial t}(\alpha,\gamma,t) < 0, \qquad t \in [t_1+\pi/2, t_1+3\pi/2]. \tag{B.3}$$

Proof. Part (a) follows from the definition of f by direct computation.

Set

$$f^{\exp}(\alpha,\gamma,t) := e^{(\gamma-\alpha)t},$$

and

$$f^{\mathrm{tr}}(\alpha,\gamma,t) := -\cos(t) + (\alpha-\gamma)\sin(t) = -\sqrt{1+(\alpha-\gamma)^2}\cos(t-t_1+\pi/2)$$

so that

$$f(\alpha,\gamma,t) = f^{\exp}(\alpha,\gamma,t) + f^{\mathrm{tr}}(\alpha,\gamma,t).$$

By inspection, both functions $f^{\exp}(\alpha,\gamma,T)$ and $f^{\mathrm{tr}}(\alpha,\gamma,T)$ are strictly convex on $[0,t_1]$, hence part (a) implies $f(\alpha,\gamma,t) > 0$ for $t \in (0,t_1]$. On the other hand, $f^{\mathrm{tr}}(\alpha,\gamma,t) \geq 0$ for $t \in [t_1, t_1+\pi]$ and $f^{\exp}(\alpha,\gamma,T) > 0$ for all $t \in \mathbb{R}$, therefore

$$f(\alpha,\gamma,t) > 0, \qquad t \in (0, t_1+\pi], \tag{B.4}$$

which proves part (b). Finally,

$$f(\alpha,\gamma,t) \leq f(\alpha,\gamma,2t_1+\pi) = -1 + f^{\exp}(\alpha,\gamma,2t_1+\pi) < 0, \quad t \in [2t_1+\pi, 2\pi],$$

and

$$\frac{\partial f^{\mathrm{tr}}}{\partial t}(\alpha,\gamma,t) \leq 0, \quad \frac{\partial f^{\exp}}{\partial t}(\alpha,\gamma,t) < 0, \qquad t \in [t_1+\pi/2, t_1+3\pi/2],$$

hence (B.3) holds, which completes the proof of part (c) and Lemma B.3. □

Lemma B.4. *Let $\alpha > 0$, $\gamma < 0$. Then,*

(a) $g(\alpha,\gamma,t) = -\frac{\gamma}{6}(1+\alpha^2)t^3 + O(t^4)$ *as* $t \to 0$*;*
(b) *if* $\alpha \geq 1$*, then* $g(\alpha,\gamma,t) > 0$ *for* $t \in (0, t_2+\pi]$*, where*

$$t_2 := \frac{\pi}{2} - \arctan\left(\frac{\alpha^2-\alpha\gamma-1}{2\alpha-\gamma}\right) \in \left(0,\frac{\pi}{2}\right); \tag{B.5}$$

(c) *if* $\alpha \geq 1$*, then* $g(\alpha,\gamma,t) < 0$ *for* $t \in [2t_2+\pi, 2\pi]$ *and*

$$\frac{\partial g}{\partial t}(\alpha,\gamma,t) < 0, \qquad t \in [t_2+\pi/2, t_2+3\pi/2]. \tag{B.6}$$

Proof. Part (a) follows from the definition of g by direct computation. Set

$$g^{\exp}(\alpha,\gamma,t) := e^{-\alpha t} - \frac{1+\alpha^2}{1+(\alpha-\gamma)^2}e^{(\gamma-\alpha)t} \tag{B.7}$$

and

$$g^{\mathrm{tr}}(\alpha,\gamma,t) := \frac{(2\alpha-\gamma)\gamma}{1+(\alpha-\gamma)^2}\cos(t) - \frac{(\alpha^2-\alpha\gamma-1)\gamma}{1+(\alpha-\gamma)^2}\sin(t) \tag{B.8}$$

$$= \frac{\gamma\sqrt{(2\alpha-\gamma)^2+(\alpha^2-\alpha\gamma-1)^2}}{1+(\alpha-\gamma)^2}\cos(t-t_2+\pi/2), \tag{B.9}$$

so that

$$g(\alpha,\gamma,t) = g^{\exp}(\alpha,\gamma,t) + g^{\mathrm{tr}}(\alpha,\gamma,t).$$

Assume that $\alpha > 1$. By inspection, the function

$$\frac{\partial^k g^{\exp}}{\partial t^k}(t,\alpha,\gamma) = (-\alpha)^k e^{-\alpha t} - (\gamma-\alpha)^k \frac{1+\alpha^2}{1+(\alpha-\gamma)^2}e^{(\gamma-\alpha)t}$$

has a unique root

$$T_k = -\frac{1}{\gamma}\ln\frac{(1+\alpha^2)(\alpha-\gamma)^k}{(1+(\alpha-\gamma)^2)\alpha^k}$$

for each $k \geq 0$. From $T_0, T_1 < 0$ and

$$e^{\alpha t}\frac{\partial^k g^{\exp}}{\partial t^k}(t,\alpha,\gamma) \to (-\alpha)^k \quad \text{as} \quad t \to \infty, \tag{B.10}$$

it follows that

$$g^{\exp}(\alpha,\gamma,t) > 0, \qquad \frac{\partial g^{\exp}}{\partial t}(\alpha,\gamma,t) < 0, \qquad t \geq 0. \tag{B.11}$$

On the other hand,

$$T_2 = -\frac{1}{\gamma}\ln\left(\frac{(1+\alpha^2)(\alpha-\gamma)^2}{(1+(\alpha-\gamma)^2)\alpha^2}\right) = -\frac{1}{\gamma}\ln\left(1-\frac{(2\alpha-\gamma)\gamma}{(1+(\alpha-\gamma)^2)\alpha^2}\right) > 0$$

and

$$T_4 - T_2 = -\frac{2}{\gamma} \ln \frac{\alpha - \gamma}{\alpha} > 0,$$

hence $T_4 > T_2 > 0$. Moreover,

$$\frac{\partial^4 g^{\exp}}{\partial t^4}(\alpha, \gamma, 0) = \frac{\alpha^4(1 + (\alpha - \gamma)^2) - (\alpha - \gamma)^4(1 + \alpha^2)}{1 + (\alpha - \gamma)^2} < 0,$$

therefore

$$\frac{\partial^4 g^{\exp}}{\partial t^4}(\alpha, \gamma, t) < 0, \qquad t \in [0, T_4),$$

i.e., the function $\frac{\partial^2 g^{\exp}}{\partial t^2}(\alpha, \gamma, t)$ is concave on the interval $[0, T_4]$, hence $T_2 < T_4$ implies

$$\frac{\partial^2 g^{\exp}}{\partial t^2}(\alpha, \gamma, t) \geq \left(1 - \frac{t}{T_2}\right) \frac{\partial^2 g^{\exp}}{\partial t^2}(\alpha, \gamma, 0) = \frac{\gamma(2\alpha - \gamma)}{1 + (\alpha - \gamma)^2} \left(1 - \frac{t}{T_2}\right) \tag{B.12}$$

for $t \in [0, T_2]$. By inspection,

$$\frac{\partial^2 g^{\mathrm{tr}}}{\partial t^2}(\alpha, \gamma, 0) = -\frac{\partial^2 g^{\exp}}{\partial t^2}(\alpha, \gamma, 0) = -\frac{\gamma(2\alpha - \gamma)}{1 + (\alpha - \gamma)^2} > 0, \tag{B.13}$$

$$\frac{\partial^2 g^{\mathrm{tr}}}{\partial t^2}(\alpha, \gamma, t_2) = 0$$

with t_2 given by (B.5), and the function $\frac{\partial^2 g^{\mathrm{tr}}}{\partial t^2}(\alpha, \gamma, t)$ is concave on the interval $[0, t_2]$, hence

$$\frac{\partial^2 g^{\mathrm{tr}}}{\partial t^2}(\alpha, \gamma, t) \geq \left(1 - \frac{t}{t_2}\right) \frac{\partial^2 g^{\mathrm{tr}}}{\partial t^2}(\alpha, \gamma, 0) = -\frac{\gamma(2\alpha - \gamma)}{1 + (\alpha - \gamma)^2} \left(1 - \frac{t}{t_2}\right) > 0 \tag{B.14}$$

for $t \in [0, t_2)$. But Lemma B.2 implies $t_2 > T_2$ and, due to (B.12) and (B.14),

$$\frac{\partial^2 g}{\partial t^2}(\alpha, \gamma, t) \geq \frac{\gamma(2\alpha - \gamma)t}{1 + (\alpha - \gamma)^2} \left(\frac{T_2 - t_2}{t_2 T_2}\right) > 0, \qquad t \in (0, T_2]. \tag{B.15}$$

Since T_2 is a unique root of the function $\frac{\partial^2 g^{\exp}}{\partial t^2}$, relations (B.10) and (B.13) imply that $\frac{\partial^2 g^{\exp}}{\partial t^2}(\alpha, \gamma, t) > 0$ for $t \in (T_2, t_2]$ and, due to (B.14) and (B.15),

$$\frac{\partial^2 g}{\partial t^2}(\alpha, \gamma, t) > 0, \qquad t \in (0, t_2].$$

By part (a) of Lemma B.4, this implies

$$g\,(\alpha, \gamma, t) > 0, \qquad t \in (0, t_2]. \tag{B.16}$$

Combining (B.11) with the relation $g^{\mathrm{tr}}\,(\alpha, \gamma, t) \geq 0$, $t \in [t_2, \pi + t_2]$, which follows from (B.9), and with (B.16), one obtains

$$g\,(\alpha, \gamma, t) > 0, \qquad t \in (0, t_2 + \pi], \tag{B.17}$$

which proves part (b). Finally, due to (B.9) and (B.11), for $t \in [2t_2 + \pi, 2\pi]$,

$$g(\alpha, \gamma, t) \le g(\alpha, \gamma, 2t_2 + \pi) = g^{\mathrm{tr}}(\alpha, \gamma, 0) + g^{\exp}(\alpha, \gamma, 2t_2 + \pi) < g(\alpha, \gamma, 0) = 0,$$

i.e.,

$$g(\alpha, \gamma, t) < 0, \qquad t \in [2t_2 + \pi, 2\pi]. \tag{B.18}$$

Moreover, relations (B.11) and

$$\frac{\partial g^{\mathrm{tr}}}{\partial t}(\alpha, \gamma, t) \le 0, \qquad t \in [t_2 + \pi/2, t_2 + 3\pi/2],$$

imply (B.6), proving together with (B.18) part (c). □

Theorem B.1. *The least positive solution $T^r(\psi) = T^r(\alpha, \gamma, \sigma, \psi)$ of Eq* (4.8) *depends continuously on the parameters $\alpha, \gamma, \sigma, \psi$ on the set*

$$D := \left\{(\alpha, \gamma, \sigma, \psi) : (\alpha, \gamma) \in D_0,\ (-\sigma, \psi) \in \mathbb{R}^2_+ \setminus (0, 0)\right\},$$

where

$$D_0 := \left\{(\alpha, \gamma) : \alpha \ge \sqrt{3}, \gamma < 0\right\} \cup \left\{(\alpha, \gamma) : 1 < \alpha < \sqrt{3},\ \gamma < \frac{\alpha(\alpha^2 - 3)}{\alpha^2 - 1}\right\}.$$

Moreover, $T^r(\alpha, \gamma, \sigma, \psi)$ is a continuously differentiable function on D.

Proof. Let us show that if $(\alpha, \gamma) \in D_0$, then $t_1 = t_1(\alpha, \gamma), t_2 = t_2(\alpha, \gamma)$ defined by (B.2), (B.5) satisfy

$$2t_2 < t_1 + \pi/2. \tag{B.19}$$

Indeed, using (B.2) and (B.5), relation (B.19) is equivalent to

$$\arctan(\alpha - \gamma) < 2 \arctan\left(\frac{\alpha^2 - \alpha\gamma - 1}{2\alpha - \gamma}\right), \tag{B.20}$$

which is true if $\alpha^2 - \alpha\gamma - 1 \ge 2\alpha - \gamma$. On the other hand, if $\alpha^2 - \alpha\gamma - 1 < 2\alpha - \gamma$, then using the double angle formula for the tangent, (B.20) is equivalent to

$$(\alpha - \gamma)\left(1 - \frac{(\alpha^2 - \alpha\gamma - 1)^2}{(2\alpha - \gamma)^2}\right) < \frac{2(\alpha^2 - \alpha\gamma - 1)}{2\alpha - \gamma},$$

i.e.,

$$2(2\alpha - \gamma)(\alpha^2 - \alpha\gamma - 1) - (\alpha - \gamma)\left((2\alpha - \gamma)^2 - (\alpha^2 - \alpha\gamma - 1)^2\right) > 0.$$

By inspection, this can be factorized as

$$\left(1 + (\alpha - \beta)^2\right)\left(\gamma + \alpha(\alpha^2 - \alpha\gamma - 3)\right) > 0,$$

therefore (B.19) holds in the parameter domain D_0.

From the definition of t_1, t_2 it follows that for $\alpha \ge 1, \gamma > 0$,

$$0 < t_1 < t_2 < \pi/2.$$

Combining this with (B.19), one obtains

$$t_1 + \pi/2 < t_2 + \pi/2 < t_1 + \pi < t_2 + \pi, 2t_1 + \pi < 2t_2 + \pi < t_1 + 3\pi/2 < t_2 + 3\pi/2,$$

therefore $[t_1 + \pi, 2t_2 + \pi]$ is a non-empty interval for any $(\alpha, \gamma) \in D_0$. Moreover, from parts (b), (c) of Lemmas B.3 and B.4, it follows that function (4.8) satisfies

$$\frac{\partial F}{\partial t}(\alpha, \gamma, \sigma, \psi, t) < 0, \qquad t \in [t_1 + \pi, 2t_2 + \pi],$$

on this interval and

$$F(\alpha, \gamma, \sigma, \psi, t) > 0, \qquad t \in (0, t_1 + \pi],$$
$$F(\alpha, \gamma, \sigma, \psi, 2t_2 + \pi) < 0$$

at its ends and outside for $(\alpha, \gamma, \sigma, \psi) \in D$, hence the conclusion of the lemma follows from the intermediate value theorem and the implicit function theorem. □

Proof of Theorem 3.2. We denote by $T^r(\mu, \psi)$ the first return time to the switching plane S from the set $\ell_-^{out} \cup \ell_+^{out} \subset \overline{S_0} \subset S$, i.e., $T^r(\mu, \psi)$ is the counterpart of $T^r(\psi)$ for system (3.33) (cf. (4.6) and (4.7)). Similarly, the counterparts of other quantities and functions defined in Sections 3 and 4, such as $\boldsymbol{w}$, $\boldsymbol{w}_0$ and the Poincaré map, depend (continuously) on μ. Under the assumptions of the theorem, from (3.25) and (3.26), it follows that $\mathrm{tr}(B(\mu)|_S) < 0$, $\det(B(\mu)|_S) < 0$ on a sufficiently small interval $\mu \in (\mu_o, \mu_*)$. Hence, the linear flow of system (3.22) continuously maps the intersection of the sliding region $\overline{S_0}$ with a sufficiently small neighborhood $\mathcal{U}$ of the point $\boldsymbol{w}_0(\mu_o)$ to ℓ_+^{out} for any $\mu \in (\mu_o, \mu_*)$, i.e., the continuous map $Q(\mu, \cdot) : \overline{S_0} \cap \mathcal{U} \to \ell_+^{out}$ is well-defined by $Q(\mu, z) = e^{T_h(\mu,z)B(\mu)}z$ with $T_h(\mu, z) := \min\{t \geq 0 : e^{tB(\mu)}z \in \ell_+^{out}\}$. Moreover, Theorem B.1 implies that for every sufficiently small $\delta > 0$ there is a $\mu^*(\delta) > \mu_o$ such that the Poincaré map (4.11) is well-defined and is continuous as the composition

$$P(\mu, \boldsymbol{w}_0(\mu) + \psi \boldsymbol{w}(\mu)) = Q(\mu) \circ \Theta_\mu(T^r(\mu, \psi), \boldsymbol{w}_0(\mu) + \psi \boldsymbol{w}(\mu)), \quad \psi \in [0, \delta],$$

of two continuous maps for each $\mu \in (\mu_o, \mu^*(\delta)]$. In other words, the function $P^c : (\mu_o, \mu^*(\delta)] \times [0, \delta] \to \mathbb{R}_+$ defined by

$$P(\mu, \boldsymbol{w}_0(\mu) + \psi \boldsymbol{w}(\mu)) = \boldsymbol{w}_0(\mu) + P^c(\mu, \psi)\, \boldsymbol{w}(\mu)$$

(cf. (4.15)) is continuous. Theorem B.1 also ensures that the point

$$z'(\mu) := \Theta_\mu(T^r(\mu, \delta), \boldsymbol{w}_0(\mu) + \delta \boldsymbol{w}(\mu))$$

depends continuously on μ on the closed interval $[\mu_o, \mu^*(\delta)]$. Recall that $\sigma(\mu_o) = 0$, $\kappa(\mu_o) > 0$. Hence, as we have seen in the proof of Theorem 3.1, the trajectory $\Theta_{\mu_0}(t, z'(\mu_o))$ proceeds along S_0 from the point $z'(\mu_o)$ either to the point

$$P(\mu_o, \boldsymbol{w}_0(\mu_o) + \delta \boldsymbol{w}(\mu_o)) = \boldsymbol{w}_0(\mu_o) + \rho\delta \boldsymbol{w}(\mu_o) \in \ell_+^{out}$$

with $0 < \rho < 1$, in which case

$$P^c(\mu_o, \delta) = \rho\delta < \delta; \tag{B.21}$$

or converges along S_0 to an equilibrium $(1 - \xi_w\delta)\boldsymbol{w}_0(\mu_o)$, i.e.,

$$\Theta_{\mu_o}(t, \boldsymbol{w}_0(\mu_o) + \delta \boldsymbol{w}(\mu_o)) \to (1 - \xi_w\delta)\boldsymbol{w}_0(\mu_o) \quad \text{as} \quad t \to \infty. \tag{B.22}$$

Due to continuity with respect to μ, relation (B.21) implies

$$P^c(\mu, \delta) \to \rho\delta < \delta \quad \text{as} \quad \mu \to \mu_o + . \tag{B.23}$$

On the other hand, since the eigenvector $\boldsymbol{w}_0(\mu_o)$ of $B(\mu_o)|_S$ corresponds to the zero eigenvalue and $\mathrm{tr}(B(\mu_o)|_S) < 0$, relation (B.22) implies

$$P^c(\mu, \delta) \to 0 \quad \text{as} \quad \mu \to \mu_o + . \tag{B.24}$$

Either of the relations (B.23) or (B.24) implies that the Poincaré map $P^c(\mu, \cdot) : [0, \delta] \to \mathbb{R}_+$ has a fixed point $\psi_\mu \in [0, \delta]$ whenever $\mu > \mu_o$ is sufficiently close to μ_o. By construction, $\Theta_\mu(t, \boldsymbol{w}_0(\mu) + \psi_\mu \boldsymbol{w}(\mu))$ is a periodic solution, which satisfies (3.35) because $\delta > 0$ is arbitrarily small. □

C. Proof of Theorem 3.3

Proof of statement (i). The case $\sigma = 0, \kappa > 0$ was considered in Theorem 3.1. If $\kappa = 0$, then the flow in S_0 is parallel to the segment L of equilibrium states according to (3.30). Hence, every non-equilibrium trajectory in S_0 reaches the set $\ell_+^{out} \cup \ell_-^{out}$ (which, in particular, implies that all the equilibrium states are unstable). Therefore, using the decomposition (A.2), if $\rho > 0$, then the Poincaré map is well-defined by (4.10)–(4.15) with $P_c(\psi) = \rho\psi$. Moreover, in this case, as in the proof of Theorem 3.1, relation (A.4) implies $\rho < 1$, consequently the iterations of the Poincaré map converge to L proving that L is an attracting set. If $\rho = 0$, then every trajectory starting from a sufficiently small neighborhood of L reaches L in finite time. If $-1 < \rho < 0$, then the Poincaré map is well-defined by (4.10)–(4.14) and (4.16) with $P_c(\psi) = \rho\psi$, and $\rho > -1$ ensures that the iterations of the Poincare map converge to L, which completes the proof of part (i).

Proof of statement (ii). Consider the closure $\overline{N(-\phi_0, \phi_0)}$ of the parallelogram (3.42) (whose diagonal is the equilibrium set L). Due to conditions (3.4) and (3.5), there is an open domain $\mathcal{U} \supset \overline{N(-\phi_0, \phi_0)}$ and a bounded function $T_1 : \mathcal{U} \to \mathbb{R}_+$ such that $\Theta(T_1(z'), z') \in \overline{S_0}$ for $z' \in \mathcal{U}$. The relations $\sigma = 0, \kappa < 0$ imply that the flow in S_0 is parallel to the vector $\boldsymbol{v}_2 = A\boldsymbol{w}$ (cf. (3.27) and (3.29)) and directed away from the straight line $\{\xi \boldsymbol{d}_0 : \xi \in \mathbb{R}\}$, which contains the equilibrium set L. Hence, every non-equilibrium trajectory leaves S_0 through the the set $\ell_+^{out} \cup \ell -^{out}$. Further, from the point $z = \boldsymbol{d}_0 + \psi\boldsymbol{w} \in \ell_+^{out}$ with a sufficiently small $\psi > 0$ (resp., $z = -\boldsymbol{d}_0 + \psi\boldsymbol{w} \in \ell_-^{out}$ with $\psi < 0$) the trajectory continues to the point $\Theta(T^r, z) = \boldsymbol{d}_0 + \psi e^{T^r A}\boldsymbol{w} \in \overline{S_0}$ (resp., $\Theta(T^r, z) = -\boldsymbol{d}_0 + \psi e^{T^r A}\boldsymbol{w} \in \overline{S_0}$). Combining the decomposition (A.2) with the identity

$$A\boldsymbol{w} = \boldsymbol{d}_0 + \phi_0 \boldsymbol{w}, \tag{C.1}$$

which follows from (3.11) and the definitions (3.40) and (3.41) of $\boldsymbol{w}$ and ϕ_0, one obtains

$$e^{T_r A}\boldsymbol{w} = \chi \boldsymbol{d}_0 + (\rho + \chi\phi_0)\, \boldsymbol{w}, \tag{C.2}$$

where due to (A.5) and (3.41),

$$\rho + \chi\phi_0 = \rho + e^{\alpha T^r} \sin(T^r)\kappa\gamma(\alpha^2 + 1) = \rho\left(1 - \frac{\kappa}{\kappa_*}\right), \tag{C.3}$$

and the assumptions $\kappa_* < \kappa < 0, \rho > 0$ imply

$$\rho + \chi\phi_0 > 0 \tag{C.4}$$

(cf. (3.39)), hence the Poincaré map is well-defined by (4.10)–(4.15) with $P^c : (-\delta, 0) \cup (0, \delta) \to \mathbb{R}$ given by $P_c(\psi) = \rho\psi$. Moreover, relations (C.1) and (C.2) imply that the trajectory starting at the corner $z_c = \phi_0 \boldsymbol{w} + A\boldsymbol{w} = \boldsymbol{d}_0 + 2\phi_0 \boldsymbol{w} \in \ell_+^{out}$ of the parallelogram $N(-\phi_0, \phi_0)$ continues to the point

$$\Theta(T^r(z_c), z_c) = \boldsymbol{d}_0 + 2\phi_0 e^{T^r A}\boldsymbol{w} = \phi_0 (2\rho - 1)\, \boldsymbol{w} + (1 + 2\phi_0\chi) A\boldsymbol{w},$$

where due to (A.6) and (C.4),

$$-\phi_0 < \phi_0 (2\rho - 1) < \phi_0, \qquad -1 < 1 + 2\phi_0\chi < 1,$$

hence

$$\Theta(T^r(z_c), z_c) \in N(-\phi_0, \phi_0), \tag{C.5}$$

and we conclude that the Poincaré map is defined on $\overline{N(-\phi_0, \phi_0)} \cap (\ell_+^{out} \cap \ell_-^{out})$, i.e., $\delta > 2\phi_0$ for $P^c : (-\delta, 0) \cup (0, \delta) \to \mathbb{R}$. Furthermore, from (C.5) it follows that all the trajectories from a sufficiently small neighborhood of L' reach L' in finite time and $\Theta(t, L') = L'$ for all $t \geq 0$, which proves part (ii) for $\kappa_* < \kappa < 0$. In the case $\kappa = \kappa_*$, relation (C.3) implies $\rho + \chi\phi_0 = 0$, hence $\Theta(T^r(z_c), z_c) = (1 - 2\rho)\boldsymbol{d}_0$, i.e., the trajectories starting on $\overline{N(-\phi_0, \phi_0)} \cap (\ell_+^{out} \cap \ell_-^{out})$ reach the interior of the equilibrium set L in finite time, and the conclusion of part (ii) follows.

Proof of statement (iii). Under the assumptions of part (iii) relation (C.3) implies $\rho + \chi\phi_0 < 0$, hence from (C.2) it follows that the Poincaré map is well-defined by (4.10)–(4.14) and (4.16). In particular, a trajectory starting at the point $z = \boldsymbol{d}_0 + \psi\boldsymbol{w} \in \ell_+^{out}$ with a sufficiently small $\psi > 0$ continues to the point

$$\Theta(T^r(z), z) = \boldsymbol{d}_0 + \psi e^{T^r A}\boldsymbol{w} = -\boldsymbol{d}_0 + \left(2\boldsymbol{d}_0 + \psi e^{T^r A}\boldsymbol{w}\right) \in S_0 \tag{C.6}$$

through the half-space Ω_+ and then, within S_0, to the point

$$P(z) = -\boldsymbol{d}_0 + P^c(\psi)\boldsymbol{w} \in \ell_-^{out} \tag{C.7}$$

along a straight line with the direction vector $-A\boldsymbol{w}$. Due to (A.2) and (C.1),

$$2\boldsymbol{d}_0 + \psi e^{T^r A}\boldsymbol{w} = (-2\phi_0 + \rho\psi)\boldsymbol{w} + (2 + \chi\psi) A\boldsymbol{w},$$

hence (C.6) and (C.7) imply that the Poincaré map is given by

$$P_c(\psi) = -2\phi_0 \operatorname{sign}(\psi) + \rho\psi, \qquad \psi \in (-\delta, 0) \cup (0, \delta),$$

where the domain is defined by $2 + \xi\psi > 0$, i.e.,

$$\delta = -\frac{2}{\chi} = -\frac{2e^{-\alpha T^r}}{\sin(T^r)}.$$

(cf. (A.5)). By inspection, $(P^c)^2$ has a fixed point $\psi^* > 0$ given by (3.45), and the assumption $\kappa^* < \kappa < 0$ is equivalent to $\psi^* \in (0, \delta)$. By assumption, $\rho > -1$ and as we know $\rho < 1$, hence ψ^* is an attracting fixed point (as is $-\psi^*$). Therefore, $L^O = \{\Theta(t, \boldsymbol{d}_0 + \psi^*\boldsymbol{w}) : t \geq 0\}$ is an attracting periodic orbit, which completes the proof of part (iii) and the theorem.